frontiers | Frontiers in Earth Science

TYPE Original Research
PUBLISHED 10 July 2024
DOI 10.3389/feart.2024.1407639

OPEN ACCESS

EDITED BY
Jens Kallmeyer,
GFZ German Research Centre for Geosciences, Germany

REVIEWED BY
Jeremy D. Owens,
Florida State University, United States
Daniel Smrzka,
University of Vienna, Austria
William Patrick Gilhooly III,
Indiana University Indianapolis, United States

*CORRESPONDENCE
Sanjukta Dhar,
Sanjukta_Dhar1@baylor.edu

RECEIVED 27 March 2024
ACCEPTED 05 June 2024
PUBLISHED 10 July 2024

CITATION
Dhar S, Frucci MN, Atchley SC and Fulton JM (2024), Spatial heterogeneity in nutrient utilization during the end-Devonian ocean anoxic event: a case study of the Western Canada sedimentary basin.
Front. Earth Sci. 12:1407639.
doi: 10.3389/feart.2024.1407639

Spatial heterogeneity in nutrient utilization during the end-Devonian ocean anoxic event: a case study of the Western Canada sedimentary basin

Sanjukta Dhar[1]*, Mason N. Frucci[1,2], Stacy C. Atchley[2] and James M. Fulton[1]

[1]Microbial Biogeochemistry Lab, Department of Geosciences, Baylor University, Waco, TX, United States, [2]Applied Petroleum Studies Lab, Department of Geosciences, Baylor University, Waco, TX, United States

The Devonian-Carboniferous (D-C; 359 Ma) boundary is marked by widespread deposition of organic-matter-rich black shales associated with the Hangenberg mass extinction event. The Exshaw Formation spans the D-C boundary in the Western Canada Sedimentary Basin (WCSB) and includes the basal Exshaw Shale deposited under broadly anoxic waters. The sediments at the base of the Exshaw Shale were deposited synchronously during a transgressive event across the WCSB, spanning the geographic variability of the basin. The variable C_{org} content of the shale was affected by local nutrient upwelling and paleotectonic features impacting water depth and circulation. To characterize the link between paleogeography and nutrient cycling, geographic (N = 20 locations) and stratigraphic (N = 6 locations) trends of $\delta^{13}C_{org}$ and $\delta^{15}N_{bulk}$ were examined throughout the WCSB, representing a range of depositional settings. The $\delta^{15}N_{bulk}$ values range between 0.0 and 6.3‰ and $\delta^{13}C_{org}$ from −29.5 to −26.8‰. Phytoplankton production in focused upwelling zones acquired a relatively ^{15}N-depleted signature through isotopic fractionation during nutrient assimilation, and the residual nutrient pool was ^{15}N-enriched. The advection of surface waters away from the location of upwelling supported additional phytoplankton growth and the deposition of sediments with higher $\delta^{15}N$ values. The stratigraphic sections include black laminated and burrowed mudrock sequences that record changes in paleoredox conditions, water depth, and tectonism over time. Up-core from the base of the Exshaw, the C_{org} content decreases and simultaneously $\delta^{15}N_{bulk}$ increases, suggesting a decrease in eutrophic conditions. Variable $\delta^{13}C_{org}$ and $\delta^{15}N_{bulk}$ trends demonstrate that there is no "type" isotopic profile spanning the D-C boundary in the WCSB.

KEYWORDS

ocean anoxia, advection model, trace element enrichment, nitrogen isotopes, black shales, nutrient cycling, Devonian, Hangenberg event

1 Introduction

Understanding biogeochemical nutrient cycles in past oceans is pivotal in reconstructing the impact of microbial life on the evolution of the earth system. Recent efforts modeling nitrogen cycling in ancient anoxic oceans have identified spatial separation in the relative contributions of NH_4^+ and NO_3^- assimilation, N_2 fixation, and denitrification to export production, all controlled by ocean circulation and local paleogeography (Higgins et al., 2012; Naafs et al., 2019). Phytoplankton populations typically draw on the pool of bioavailable nutrient-N consisting of mainly NO_3^- in oxygenated waters and NH_4^+ where anoxia occurs in the photic zone. Where the water is suboxic, the NH_4^+ pool is upwelled to overlying oxygenated waters where it is nitrified (Fernandez and Farias, 2012; Dalsgaard et al., 2012). Nitrogen fixation is focused in regions where N-nutrients (NO_3^- and NH_4^+) are depleted, and bioavailable phosphorus remains. This study applies these findings of global-scale nutrient dynamics modeling to a regional examination of N utilization in the Western Canada Sedimentary Basin (WCSB) during the Devonian-Carboniferous (D-C) transition.

Atmospheric N_2 fixed by diazotrophic cyanobacteria maintains phytoplankton growth in the ocean, compensating for bioavailable nutrient-N lost to denitrification and anaerobic ammonium oxidation (anammox) processes (Zehr and Ward, 2002; Altabet, 2005; Kuypers et al., 2018; Pajares and Ramos, 2019). The N isotopic composition of phytoplankton generally reflects the balance between assimilation of nutrient-N that is ^{15}N-enriched by denitrification and anammox, and N_2 fixation that results in low δ^{15}N values in biomass. Complete uptake of available N-nutrients will transfer the isotopic composition of the initial nutrient pool to plankton biomass. However, partial utilization of available nutrients results in N isotopic fractionation, wherein the biomass is relatively ^{15}N depleted and the residual nutrient pool enriched in ^{15}N. This is due to the preferential incorporation of lighter nitrogen (^{14}N) into the phytoplankton cells. Subsequent phytoplankton growth using the residual nutrient pool yields biomass that is ^{15}N enriched relative to the initial biomass, and advective surface water currents can cause spatial separation of low and high δ^{15}N OM (e.g., De Pol-Holz et al., 2009). Applying Rayleigh fractionation, we can explain the spatial trends in δ^{15}N across different productivity regimes in WCSB.

In modern oceans, the deep nutrient pool forms through decomposition of sinking particulate organic matter (OM), with NH_4^+ produced by ammonification and NO_3^- by nitrification under oxidizing conditions (Stief, 2013). Deep waters are brought up to the surface where meridional winds promote advection, surface water divergence, and equatorial and coastal upwelling. Thus, nutrient-rich waters are upwelled near the equator and on the tropical/subtropical western margins of continents such as the Peruvian margin, California coast, southern and northwest Africa, and Arabian Sea in the modern ocean (Kumar et al., 2001; Altabet et al., 2002; Kienast et al., 2002; Altabet, 2005; Elfi Mollier-Vogel et al., 2012). The upwelled nutrients support phytoplankton growth in the photic zone (Carbonel and Valentin, 1999; Reyes-Mendoza et al., 2019). Enhanced primary production and export on continental margins leads to oxygen consumption by respiration below the photic zone, and slow ventilation of subsurface water creates oxygen minimum zones (OMZs) that can expand into widespread ocean anoxia (Karstensen et al., 2008; Jenkyns et al., 2010; Schönfeld et al., 2015). Bottom water anoxia/suboxia promotes the preservation of phytoplankton δ^{15}N values, especially in relatively shallow water and adjacent to continental margins (Calvert et al., 1996).

Broad shifts in nutrient speciation and concentration during the Paleozoic were closely tied to changes in delivery from terrestrial sources, marine primary production, OM decomposition, and deep-water ventilation (Saltzman, 2005; Liu et al., 2016; Naafs et al., 2019; Pajares and Ramos, 2019). Major changes in ocean biogeochemistry were linked to excursions in carbon and nitrogen isotopic compositions, identifiable through geochronologic analyses of sedimentary records. The biogeochemical shifts associated with the D-C boundary (359 Ma) have been connected to the Hangenberg mass extinction. This event has been recognized globally, including end-Devonian sediments from the Rhenish Massif in the Rhenohercynian Basin, Germany (Kaiser et al., 2006), Carnic Alps in Carnic Basin, Italy (Bábek et al., 2016), Namur-Dinant Basin in Belgium and northern France (Kumpan et al., 2015), Holy Cross Mountains in the Polish Basin (Matyja et al., 2021), Witpoort Formation, South Africa (Scholze and Gess, 2017), and Cat Ba Island in Vietnam (Komatsu et al., 2014). In North America, End-Devonian black shales from Iowa, Missouri, Illinois, North Dakota, and Ohio in the United States and the WCSB in Alberta are correlated chronostratigraphically with other global Hangenberg intervals (Schmoker and Hester, 1983; Robison, 1995; Caplan and Bustin, 1998; Myrow et al., 2011; Martinez et al., 2019). At most locations, the D-C boundary features a succession of OM-rich black shales, calcareous shales, and limestones related to glacioeustatic sea-level oscillation (Pisarzowska et al., 2020).

The stratigraphic correlation of Late-Devonian OM-rich black shales from epicontinental basins suggests a link between marine export production and mass extinction (Caplan and Bustin, 1999; Kaiser, 2005; Becker et al., 2016a). Paleontological data from these sediments indicates the loss of >50% of marine biodiversity, including ammonoid, trilobite, conodont, fish, acritarch, and foraminifera taxa (Becker et al., 2016b). The extensive black shale record representing the Late-Devonian mass extinction is indicative of a gradual and episodic environmental transformation rather than a cataclysmic one, resulting in a series of extinction events over a period of ~15 Ma. The proliferation of vascular land plants was a bioevolutionary mechanism that triggered a cascading effect of associated environmental changes during the Devonian Period. With increased root biomass that penetrated greater depths into the soil, the rates of continental weathering and nutrient flux to the ocean were exacerbated and led to nutrient cycle perturbations in the ocean (Algeo and Scheckler, 2010; Marynowski et al., 2012; Liu et al., 2016; Zhang et al., 2020). This eventually led to expanded marine anoxia, which caused a global marine mass extinction event. The enhanced continental weathering and high rates of carbon burial were also responsible for a shift from a greenhouse climate of the Devonian to an icehouse climate in the Carboniferous (Kaiser et al., 2016; Rakociński et al., 2020; Heath et al., 2021).

During the D-C transition, the WCSB was a shallow epicontinental sea along the tropical western margin of the North American Craton (Blakey, 2008). The sediments deposited during this time comprise the Banff Assemblage. The WCSB was bounded

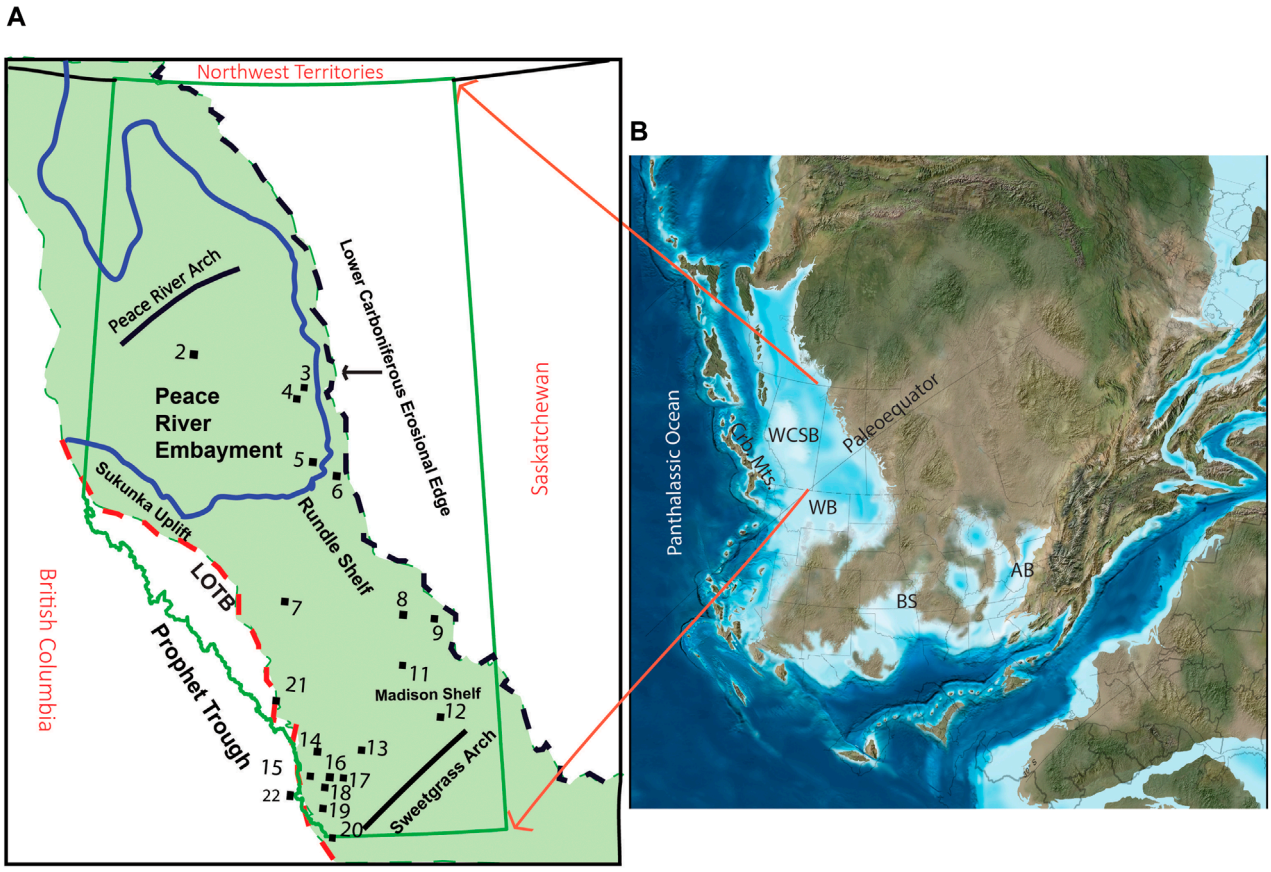

FIGURE 1
(A) Geographic extent of the Banff Assemblage shaded in green and sample locations. LOTB = Laramide Orogeny Thrust Belt **(B)** Devonian paleogeography: WCSB, Western Canada Sedimentary Basin; WB, Williston Basin; Crb. Mts., Cariboo Mountains; BS, Burlington Shelf; AB, Appalachian Basin [Modified from Blakey (2008) and Barclay et al. (1994)].

by the Peace River Arch to the north, the North American Cratonic margin to the east, the Prophet Trough to the west, and the Sweetgrass Arch to the southeast. The Sweetgrass Arch also separated the WCSB from the contemporaneous Williston Basin (WB, Figure 1). North of the Antler orogenic belt and west of PT, the Cariboo mountains formed due to Mid-Devonian contractional deformation in the Cordilleran margin (Smith et al., 1993; Barclay et al., 1994). Post deposition, the Banff Assemblage was truncated to the east by the Lower Carboniferous erosional edge and to the west by the Laramide Orogeny fold and thrust belt (Figure 1). The tropical location of the WCSB on the western margin of the North American Craton promoted surface water divergence and coastal and equatorial upwelling of nutrient-rich waters that supported elevated primary productivity and export production to the sediments (Parrish, 1982; Robison, 1995).

Nitrogen isotope records from oceanic anoxic events (OAEs) commonly register low $\delta^{15}N$ signals, usually attributed to diazotrophy and NH_4^+ assimilation. This study uses $\delta^{13}C_{org}$, $\delta^{15}N_{bulk}$, C_{org} weight percent, and redox-sensitive trace element enrichment factors to assess variable nutrient dynamics across an epicontinental basin. Regional tectonism and global eustasy led to basin-wide spatial heterogeneity in water depth and sedimentation rates (Robison, 1995; Caplan and Bustin, 1999). The interaction between upwelling zones supporting high primary productivity and regions of stable density stratification inhibiting mixing affected variable OM export to the sediments (Caplan and Bustin, 1998; 2001; Murphy et al., 2000; Werne et al., 2002; Ross and Bustin, 2008; Tuite et al., 2019; Kabanov and Jiang, 2020). For the WCSB, we hypothesize that the incomplete utilization of nutrients in upwelling zones and variable utilization of nutrients and N_2 fixation along the flow path of advected surface waters resulted in progressively lower export production and increasing $\delta^{15}N$ values. These variations make the WCSB an ideal setting to study the effects of local paleogeography on marine biogeochemical cycle processes and OM accumulation. It further establishes a mechanism for local variability in nutrient cycling and primary productivity from the WCSB that captures the dynamics of the global marine N cycle during periods of intense ocean anoxia.

2 Methods

2.1 Preparation of samples

Fresh specimens for geochemical analysis were collected from sediment cores at the Alberta Energy Regulator Core Research

Centre (Calgary, Alberta, Canada). Cores were described to identify sedimentary facies and formation unit boundaries, which were differentiated based on ichnology, bioturbation intensity, grain size, fossil prevalence, reactivity to 10% HCl, fracture frequency, sedimentary structures, and color (Frucci, 2021). The cores were then depth-corrected to match log depth by comparing core-observed rock attributes and gamma-ray, induction, and neutron/density log response (Visy, 2022). Additional samples from two outcrop exposures of the Exshaw Formation at Jura Creek and Crowsnest Pass (Locations 21 and 22, Figure 1) were also analyzed in this study. For each outcrop sample, exposed/weathered surfaces were removed using a grinder before being broken into small chips using a rock hammer and powdered in a shatterbox (SPEX Industries Inc., Catalog No. 8500). For C and N isotopic analysis, the powdered samples were decarbonated using 10% HCl (v/v) for 48 h and centrifuged at 3000 RCF for 4 min. The supernatant was then decanted, and acid was added to test for effervescence that indicates residual inorganic carbon. After decarbonation, samples were rinsed three times or until pH neutral with deionized water, centrifuged, and the supernatant discarded. The solid residue was dried using a freeze drier for 24–48 h.

2.2 Bulk stable isotope analyses

For determination of bulk $\delta^{13}C_{org}$ and $\delta^{15}N_{bulk}$, 10–30 mg decarbonated samples were weighed into tin capsules and loaded into a zero-blank auto-sampler on an elemental analyzer (EA; Costech, ECS 4010) coupled with an isotope ratio mass spectrometer (IRMS; Thermo-Electron Delta V Advantage) in the Baylor Geosciences Stable Isotope Lab. We analyzed the N isotopic composition of a set of 8 non-acidified Exshaw Shale samples to examine the effect of acidification on $\delta^{15}N$ values. On average the acidified samples were ^{15}N-enriched by 0.68 ± 0.69‰. While this difference is not trivial, the geographic and stratigraphic trends are captured by the $\delta^{15}N$ values of acidified samples. The N_2 and CO_2 produced in the EA passed through a thermal conductivity detector for total nitrogen and organic carbon determination prior to transfer to the IRMS. Samples were analyzed in batches of 10 bracketed by blanks and an internal standard acetanilide calibrated to international isotope standards (USGS 40: $\delta^{13}C$ = −26.39‰, $\delta^{15}N$ = −4.52‰; USGS 41: $\delta^{13}C$ = +37.63‰, $\delta^{15}N$ = +47.57‰). Isotopic composition is reported in conventional δ notation relative to Vienna Pee Dee Belemnite (VPDB) for carbon and atmospheric N_2 for nitrogen. Standard deviations range between 0.01 and 0.1‰ for $\delta^{13}C_{org}$ and 0.12–0.24‰ $_{for}$ $\delta^{15}N$.

2.3 Trace element analysis

Trace and major element concentrations were measured using a portable Bruker TRACER 5i X-Ray Fluorescence (XRF) spectrometer. To assess redox conditions, vanadium, molybdenum, uranium, nickel, chromium, and cobalt concentrations are reported and normalized to aluminum to account for terrigenous inputs of the trace elements (TE). Four standards, Zentrales Geolosches Institut *Black Shale* (ZGI TS), Mintek *Carbonaceous Shale* (SARM 41), Geological Survey of Japan *Black forest soil* (JSO-1), and Geological Survey of Japan *Porites* sp. *Coral* (Jcp-1), were analyzed before and after each batch of samples for a total of 10 replicates. These values were used to determine accuracy and precision of analyses and calculate response factors to assess the stability of the internal "Mudrock" calibration. For ZGI TS, the relative uncertainty (1σ standard deviation) calculated during analysis was 10.5% for Al, 3.8% for V, 3% for Mo, 18.7% for U, 5.8% for Ni, 13% for Co, and 5.3% for Cr. Trace element enrichment factors (EF) were calculated relative to the reference elemental concentration values reported for the global average Post-Archean Australian Shale (PAAS) (Taylor and McLennan, 1985; Tribovillard et al., 2006; Algeo and Liu, 2020).

3 Results

The C_{org} concentration for decarbonated sediments ranged between 0.3% and 19.9%, with a maximum typically at or near the base of the Exshaw Fm. (Figure 2). We report stratigraphic profiles of $\delta^{13}C_{org}$ and $\delta^{15}N_{bulk}$ for three depositional provinces: the Peace River Embayment (PRE; Loc. 3 and 4 on Figures 1, 2A,B), the Madison Shelf (Loc. 9 and 11 on Figures 1, 2C,D) and the eastern margin of the Prophet Trough (Loc. 21 and 22 on Figures 1, 2E,F). The Exshaw Fm. consists of shale and siltstone members that unconformably overlie earlier Famennian carbonate rocks (Caplan and Bustin, 1998; Vernon, 2001; Stoyles et al., 2011). The study interval stratigraphically comprises five units: (1) the Big Valley or Palliser Fms. at the base (carbonate skeletal packstone or laminated nodular sediments), (2) the Exshaw Lower Shale (fine-grained laminated or burrowed black mudstone), (3) the Exshaw Upper Shale (mechanically laminated mudstone or burrowed mudstone), (4) the Exshaw Siltstone (mechanically laminated siltstone), and (5) the Banff Fm. (variable components of black laminated mudstone, interbedded carbonate/black mechanically laminated mudstone, or skeletal packstone; Frucci, 2021; Visy, 2022). The Exshaw Lower Shale unit is C_{org}-rich with little carbonate content, and the Upper Shale is calcareous with decreased C_{org} content (Richards and Higgins, 1988; Savoy, 1990; Smith et al., 1995; Vernon, 2001).

3.1 Carbon profiles

The Peace River Embayment was a prominent bathymetric feature of the WCSB at the end of the Devonian and served as a relatively deep-water connection between the open ocean and Prophet Trough to the basin's interior (Robison, 1995). At Loc. 3 and 4, the C_{org} content increased from ~0.4% in the Big Valley (BV) Fm. to 6.1% and 11.7%, respectively, at the base of the Exshaw Fm. (Figures 2A,B). The average C_{org} content at Loc. 4 decreased up-core from 5.7% ± 1.6% in the Exshaw Shale to 3.3% ± 0.2% in the Banff Fm. The $\delta^{13}C_{org}$ values decreased from −28.4‰ in the BV to −28.6 ± 0.2‰ in the Exshaw Shale, −29.2 ± 0.4‰ in the Siltstone, and −29.1 ± 0.1‰ in the Banff Fm. At Loc. 3, a consistent C_{org} content of 5.2% ± 0.7% and $\delta^{13}C_{org}$ of −28.8‰ was maintained throughout the shale and siltstone units. A similar published profile for the Peace River Embayment near Loc. 2 (Figure 1) reported $\delta^{13}C_{org}$ values between −28.2 and −28.5‰ across the Exshaw interval (Caplan and Bustin, 1998).

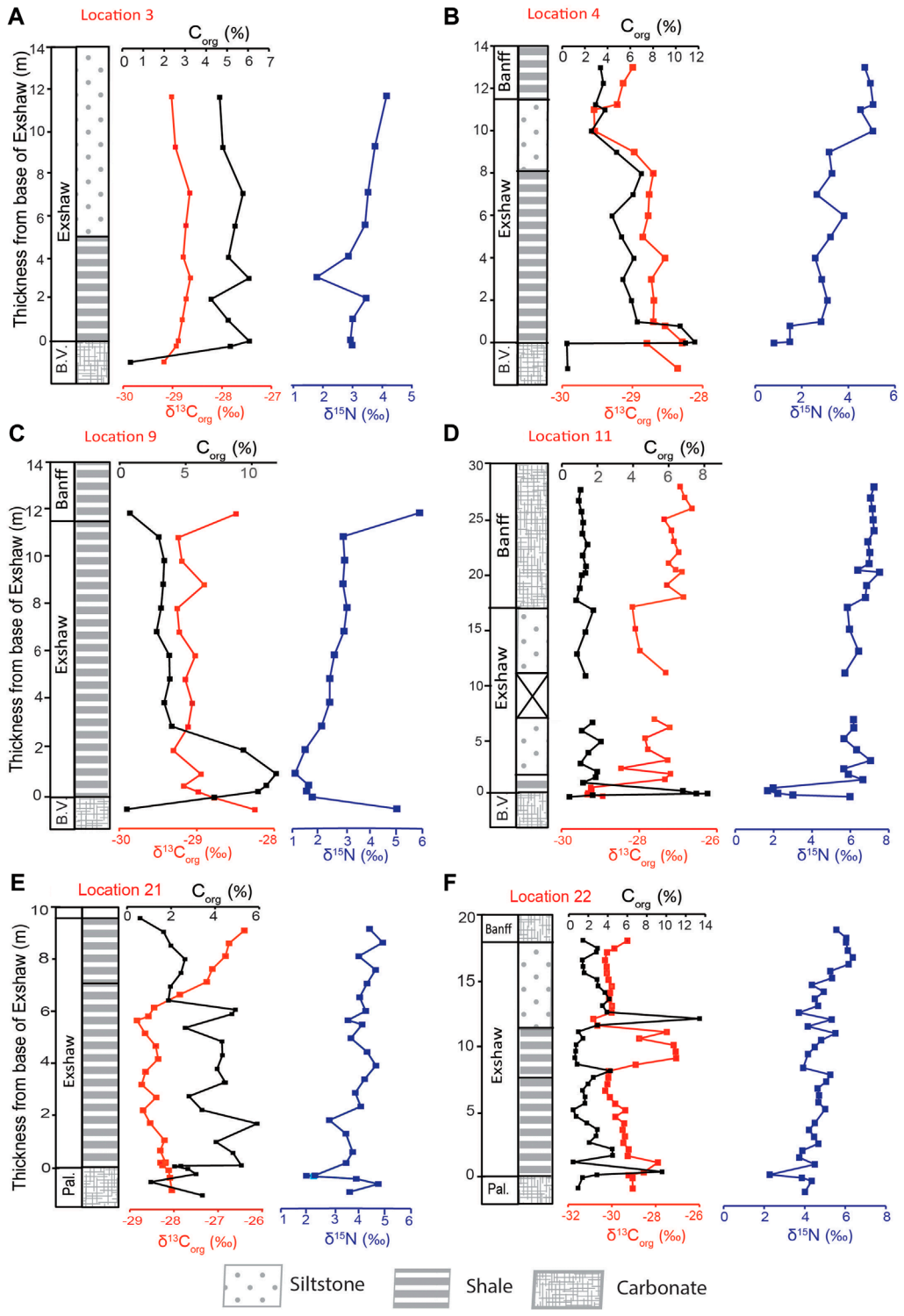

FIGURE 2
Stratigraphic profiles of C_{org} and bulk N isotopic compositions for Banff Assemblage sediments from the Peace River Embayment [**(A)** Loc. 3; **(B)** Loc. 4], Rundle Shelf [**(C)** Loc. 9; **(D)** Loc. 11], and Prophet Trough [**(E)** Loc. 21; **(F)** Loc. 22]. Abbreviations: Pal., Palliser Formation; B.V., Big Valley Formation.

The Loc. 11 core includes the Big Valley carbonate at the base, a very thin layer of Exshaw Shale (~1.25 m) overlain by siltstone and Banff carbonate (Figure 2D). In comparison, the Exshaw Shale at Loc. 9 is 10.75 m thick without a siltstone member above it (Figure 2C). These two locations occur on the Madison Shelf, which was a shallow marine setting compared to the Peace River Embayment in the north and the Prophet Trough in the west (Smith and Bustin, 2000; Vernon, 2001). At Loc. 11, C_{org} increased from 0.4% just below the Exshaw Fm. to a maximum of 8.2% in the Exshaw shale. The average C_{org} content decreased rapidly thereafter,

to < 2% in both the Exshaw Siltstone and Banff Fm. Average $\delta^{13}C_{org}$ value increased from −29.3 ± 0.1‰ in the Exshaw Shale to −27.7 ± 0.4‰ to −27.0 ± 0.2‰ in the Banff Fm. At Loc.9, C_{org} increased from 0.5% in the BV Fm. to a maximum of 10.5% near the base of the Exshaw Shale. It then decreased to 0.8% in the Banff Fm. The $\delta^{13}C_{org}$ values of Exshaw Shale at Loc.9 were similar to Loc. 11 despite differences in unit thickness. At Loc. 9, average $\delta^{13}C_{org}$ values of Exshaw Shale was −29.1 ± 0.1‰ and rose to −28.5‰ in the Banff Shale.

The Banff Fm. sediments at Jura Creek (Loc. 21) and Crowsnest Pass (Loc. 22) were deposited along the eastern margin of the Prophet Trough. Here, the Palliser Fm. underlies the Exshaw Fm., and the Exshaw Shale is formally divided into Lower Shale and Upper Shale members based on their C_{org} richness, microfossil abundance and mineral content (Vernon, 2001). Both shale members consist of black laminated mudrocks, but the Lower Shale had a higher C_{org} content. At Loc. 21, the average C_{org} concentration for the Lower Shale was 3.9% ± 1.1% and the Upper Shale was 1.9% ± 0.7%. There was a drop in $\delta^{13}C_{org}$ values from −28.3‰ to −28.9‰ in the Lower Shale, followed by a ^{13}C enrichment to −26.5‰ in the Upper Shale (Figure 2E). At Loc. 22, the C_{org} content for the Lower Shale ranged between 0.5% – 9.6%, with a mean C_{org} of 2.8% ± 2.4%, whereas for the Upper Shale, it ranged between 1.4% and 4.3%, and a mean C_{org} of 2.6% ± 1.1% was recorded. There was a notable maximum of 13.4% at the base of the siltstone unit (Figure 2F). $\delta^{13}C_{org}$ values ranged from −29.4‰ at the base of the Exshaw to −27.2‰ in the siltstone member. The occurrence of a ~3‰ ^{13}C-enrichment at the transition from the Lower to Upper Shale at both Loc. 21 and 22 is notable, as this is the most significant carbon isotopic excursion detected in the WCSB.

3.2 Nitrogen profiles

Banff Assemblage $\delta^{15}N$ profiles were broadly similar at all locations, exhibiting relatively low values (0.1–2.9‰) at or near the base of Exshaw Shale associated with high C_{org} content (Figure 2). The maximum $\delta^{15}N$ values ranged between 4.5‰ and 7.2‰, corresponding with lower C_{org} near the top of the cored intervals. In the Peace River Embayment at Loc. 4, the $\delta^{15}N$ minimum of 1.5‰ was at the base of the Exshaw Shale, and the average was 2.8 ± 0.6‰ for the Shale and 4.0 ± 0.9‰ for the Exshaw Siltstone. The overlying Banff Fm. had an average $\delta^{15}N$ value of 4.9 ± 0.2‰. A previous investigation by Caplan and Bustin (1998) at a site close to Loc. 2 reported $\delta^{15}N$ with a stratigraphic trend similar to that at Loc. 4, with a minimum of 0.5‰ at the base of Exshaw and increasing upward to a maximum of 5.1‰. At Loc. 3, there was a gradual increase in $\delta^{15}N$ from 2.9‰ at the Exshaw base to a maximum of 4.2‰ in the siltstone unit. The average $\delta^{15}N$ value was 3.2 ± 0.6‰ for Exshaw Shale and 3.7 ± 0.2‰ for Siltstone.

The two Madison Shelf locations recorded 3–4‰ negative $\delta^{15}N$ excursions across the Big Valley/Exshaw Boundary and positive excursions of similar magnitude at the top of the Exshaw Shale (Figures 2C,D). Loc. 9 had a minimum $\delta^{15}N$ value of 1.6‰ near the base of the Exshaw Fm., an up-core increase to 3.0‰ near the Exshaw top, and a maximum of 5.9‰ at the bottom of Banff Fm. The average $\delta^{15}N$ for the Exshaw Shale was 2.4 ± 0.7‰. There was a positive trend in $\delta^{15}N$ values up-core at Loc. 11 from 1.9 ± 0.3‰ in the Exshaw Shale to 7.0 ± 0.3‰ in the Banff Fm.

Locations 21 and 22 also had positive up-core trends in $\delta^{15}N$ (Figures 2E,F), recording a ~2‰ negative excursion at the Exshaw base, with a minimum of 2.1 and 2.2‰, respectively. Loc. 21 had an average $\delta^{15}N$ of 3.7 ± 1.1‰ for the Lower Shale and 4.5 ± 0.8‰ for the Upper Shale. At Loc. 22, average $\delta^{15}N$ values increased from 4.6 ± 0.3‰ for the Lower Shale to 6.2‰ for one sample in the Banff Fm.

3.3 Carbon and nitrogen at the base of the Exshaw

Sediments from the base of the Exshaw Shale had an average C_{org} concentration of 7.9% ± 5.9% across 20 locations. There was significant variability among sites, with the greatest C_{org} content at Loc. 2 (19.9%) in the Peace River Embayment, Loc. 5 (18.6%) on the northern edge of the Rundle Shelf, and Loc. 17 (18.4%) on the Madison Shelf (Figure 3). Low C_{org} content was found at Loc. 6 (0.7%) on the Rundle Shelf and Locs. 15 (0.3%), 16 (0.2%), and 18 (2.0%) on the southwestern edge of the Madison Shelf adjacent to the Prophet Trough. The $\delta^{13}C_{org}$ values ranged between −29.5 and −26.8‰ across the basin, with low C_{org} locations having relatively ^{13}C-enriched (−27.8 ± 0.7‰) OM compared with the moderate (−28.9 ± 0.4‰) and high (−28.6 ± 0.6‰) C_{org} locations (Figure 4). The $\delta^{15}N$ values at the base of the Exshaw Shale ranged from 0.0 to 6.3‰ and were inversely correlated with C_{org} content (Figures 3, 4). Locations with low C_{org} content were most ^{15}N-enriched ($\delta^{15}N$ = 6.0 ± 0.5‰) compared with locations with moderate (2.4 ± 1.1‰) and high (0.5 ± 0.1‰) C_{org} content.

3.4 Trace element enrichment at the base of the Exshaw

The Exshaw Shale member has consistently higher concentrations of redox-sensitive TEs relative to the underlying and overlying strata (Supplementary Figure S1; Frucci, 2021). Trace elements are relatively immobile irrespective of the level of catagenesis (Ross and Bustin, 2008), so spatial trends in their enrichments reflect geographic variability in redox conditions during deposition and early burial (Pi et al., 2014; Algeo and Liu, 2020). We focused our analysis on samples from the base of the Exshaw Shale to compare spatial patterns in redox conditions with C and N stable isotope distributions during a single time interval when transgression created sediment accommodation space throughout the depositional basin (Figure 3). We found greater than two orders of magnitude difference in EFs across the basin (Table 1). The ratios of Mo, U, and Ni to Al for all sampled locations were greater than those of the reference PAAS, with maximum EFs of 3.0×10^3 for Mo, 4.5×10^2 for U, and 1.3×10^3 for Ni at Loc. 14 and similarly high EFs at Loc. 19 (Figure 3; Table 1). The Zn_{EF} and Co_{EF} were also elevated at Locs. 14 and 19, but at many locations Zn_{EF} and Co_{EF} was <1.0 indicating content similar to and below that of PAAS (Table 1). The V_{EF} was >1.0 at all locations except one, and it was greatest at Locs. 14 and 17. The Cr_{EF} ranged only between 0.52 and 3.14, and the Cr concentration was below the level of detection at Locs. 13, 14, 16, 18, and 19 in the south of the WCSB.

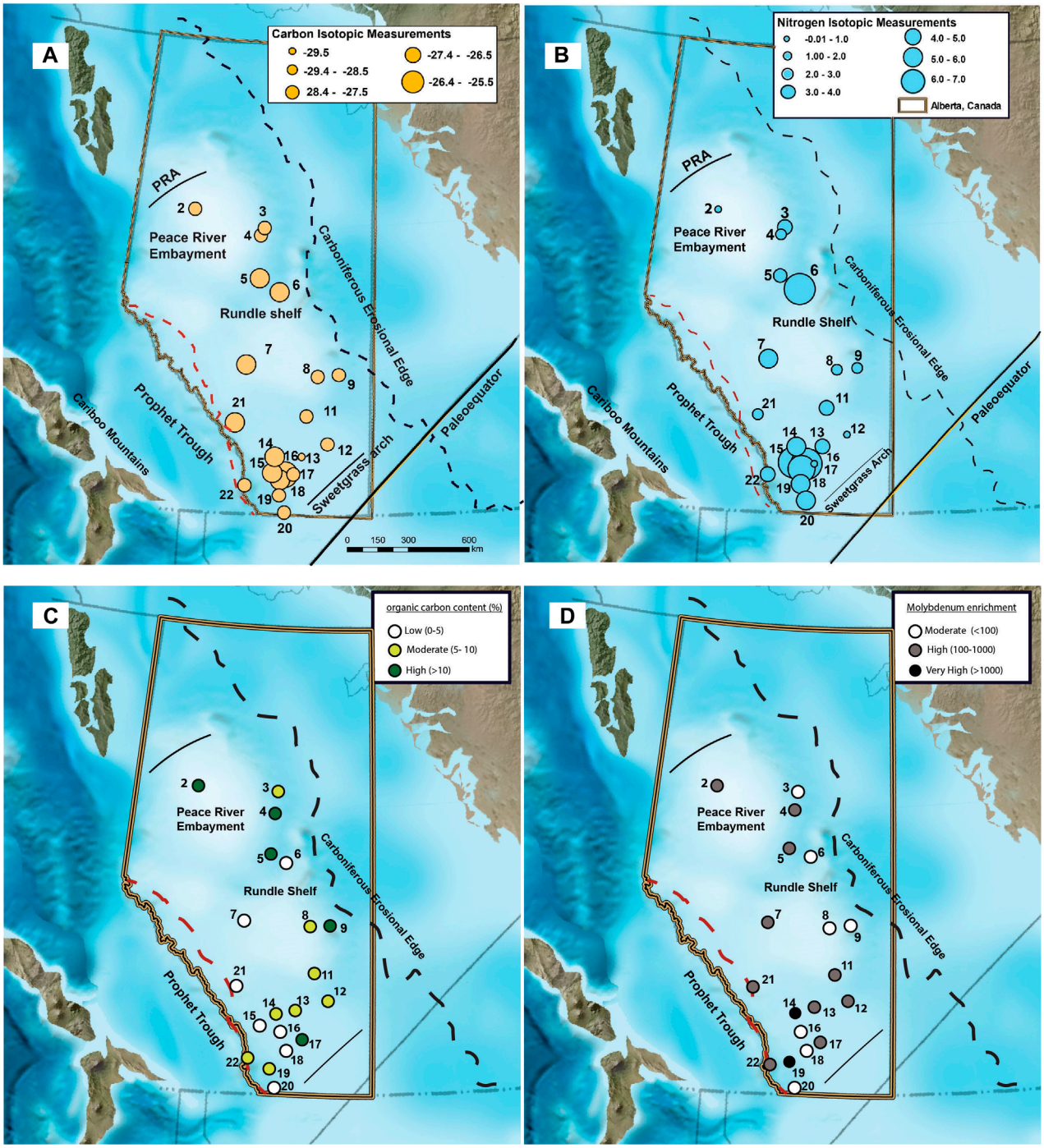

FIGURE 3
Spatial distribution of **(A)** $\delta^{13}C_{org}$, **(B)** $\delta^{15}N$, **(C)** C_{org} (%), and **(D)** Mo enrichment at the Exshaw base across the Western Canada Sedimentary Basin [Modified from Blakey (2008)].

There is a general pattern of covariance among the TEs at the base of the Exshaw Shale as shown by the positive Spearman rank order correlation coefficients (r; Figure 5). Elevated Mo_{EF} and U_{EF} in black shales are commonly used to infer bottom water anoxia (Algeo and Li, 2020), and are strongly correlated at the base of the Exshaw Shale ($r = 0.84$, $p < 0.001$). Strong correlation with Mo_{EF} was also observed for Ni_{EF}, Zn_{EF}, and V_{EF} (Figure 5; Supplementary Figure S2), all with $p < 0.001$). The Cr_{EF}

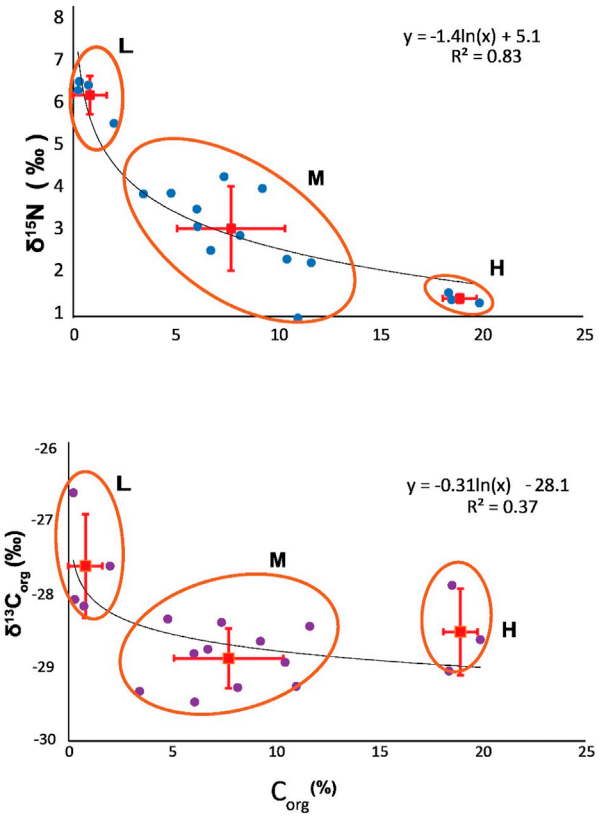

FIGURE 4
Three groups of locations with high (H: 19.0% ± 0.8%), moderate (M: 7.7% ± 2.6%), and low (L: 0.8% ± 0.8%) C_{org} at the base of the Exshaw and an inverse relationship between C_{org} content and $\delta^{15}N_{bulk}$. A natural logarithmic curve to the $\delta^{15}N$ vs. C_{org} data (R^2 = 0.83) indicates Rayleigh fractionation of N isotopes between the highly productive regions and nutrient-limited distal locations. Error bars indicate standard deviation (1σ) from the mean values of C_{org}, $\delta^{15}N$, and $\delta^{13}C$.

was weakly correlated with Mo_{EF} (r = 0.57, p = 0.033), and Co_{EF} was not significantly correlated with Mo_{EF} (p > 0.05). Devonian-Carboniferous black shales deposited in other North American basins are also highly enriched in Mo and U, with molar ratios of Mo to U ranging from 0.4 to 2 times the seawater molar ratios (Algeo and Tribovillard, 2009), and variable sedimentation rate and dilution by detrital minerals can explain variable enrichment of TEs deposited at that time (Algeo and Liu, 2020). The thickness of the Exshaw Shale interval in the WCSB, however, was not significantly correlated with any TE enrichment factors (Figure 5). Considering shale member thickness as a proxy for sedimentation rate, with a greater rate inferred for thicker intervals, the spatial variation in the degree of enrichment likely reflects differences in ocean redox conditions or circulation patterns across the basin. Paleogeographic reconstructions indicate that shallower regions on the eastern boundary of the Peace River Embayment, the eastern Rundle Shelf, and the southwestern Madison Shelf generally experienced lower TE enrichment (Figure 3D). Locations with greater enrichment of TEs, especially V and Mo (Figure 5), typically corresponded to greater C_{org} content (Figures 3C,D), though the relationship was relatively weak suggesting other controls such as primary productivity were more influential on C_{org}.

4 Discussion

4.1 Geographic variability in biogeochemical cycling processes in the WCSB

The onset of Exshaw Shale deposition was tied to the first of three transgressive events recorded in the Famennian-Tournaisian Banff assemblage (Smith and Bustin, 2000), which spans the D-C boundary in the WCSB (Macqueen and Sandberg, 1970). Crustal deformation associated with the Antler Orogeny, active during the Late Devonian and Carboniferous, produced the relatively complex seafloor bathymetry of the WCSB (Jewell, 1994; Robison, 1995). The intense tectonic activity affected the entire western extent of the North American craton, and in the WCSB it caused deepening of the Prophet Trough and parts of the cratonic platform and shelf margin (Poole, 1973; Savoy, 1990; Barclay et al., 1994; Smith et al., 1995). Crustal extension and vertical fault block movement also resulted in deepening of the Peace River Embayment (Caplan and Bustin, 2001; O'Connell et al., 1990). Thicker deposits of the Exshaw Shale accumulated on descending blocks as deeper locations had greater depositional accommodation (Smith et al., 1995; Smith and Bustin, 2000; Zaitlin, 2011; Visy, 2022). The difference in shale thickness and therefore sediment accumulation rate, for example, at Loc. 9 compared with Loc. 11, did not result in a dilution effect on geochemical characteristics (Figures 2, 5).

The complex bathymetry of the WCSB, which extended from the paleo-equator to ca. 10° N, likely affected the location of bottom water currents and regions of upwelling (Caplan and Bustin, 1998). On modern tropical western continental margins, interactions among wind stress, Ekman transport, and basin geometry can produce focused regions of surface water divergence and upwelling (Brandt et al., 2023). The WCSB likely included regions within the Peace River Embayment where upwelling was favored. As a modern geographical analog to the WCSB, the tropical seas between Indonesia and Australia have similar complex bathymetry. A study of the Arafura Sea modeled subsurface currents and related the complex bathymetry with the upwelling of nutrient-rich water near the shelf break, where there is elevated primary productivity (Kämpf, 2016). Subsequently, the newly upwelled waters become relatively nutrient-depleted, and these residual waters advect via surface currents to less productive regions.

Similar effects of bathymetry, currents, and upwelling on primary productivity can explain the spatial variability in C_{org} content of the Exshaw Shale. Greater C_{org} content is associated with eutrophic locations, and relatively oligotrophic (or less eutrophic) locations have lower C_{org} content (O'Connell et al., 1990; Richards, 1989). Based on Rock-Eval pyrolysis hydrogen index (Supplementary Table S1), OM in the Exshaw Fm. at all locations throughout the WCSB was principally derived from marine organisms. Short chain alkanes basin-wide also indicate the dominance of marine-derived OM (Frucci, 2021). The greater C_{org} content at the base of the Exshaw Fm. reflects increased primary productivity and export production coinciding with the transgressive stratal succession at the onset of black shale deposition (Caplan and Bustin, 2001; Visy, 2022). The broad distribution of marine sourced OM agrees with the previous analysis of

TABLE 1 Trace metal EFs for samples from the base of Exshaw Fm. for 20 locations across WCSB.

Locations	Mo_{EF}	U_{EF}	V_{EF}	Ni_{EF}	Cr_{EF}	Co_{EF}	C_{org}(%)
2	164	35.9	4.94	4.91	1.02	0.67	19.9
3	67.7	28.1	1.39	2.37	0.52	0.72	5.2
4	155	22.3	4.33	4.43	1.05	0.76	11.7
5	436	78.9	8.68	12.7	1.38	<LOD	18.6
6	39.1	11.8	1.80	2.32	0.84	0.58	0.7
7	106	32.1	5.26	5.31	0.88	1.17	4.8
8	45.3	<LOD	2.67	6.89	1.83	6.19	6.7
9	78.9	21.1	2.18	4.03	0.80	1.23	10.5
11	110	22.4	2.74	7.15	1.14	1.05	8.2
12	268	62.9	11.0	15.3	2.16	2.68	11.0
13	276	33.9	4.53	6.01	<LOD	1.95	6.1
14	3,004	451	22.8	1,272	<LOD	33.2	7.4
15	<LOD	130	1.60	7.29	3.14	<LOD	2.0
16	17.9	<LOD	0.54	2.00	<LOD	1.59	0.2
17	598	65.3	30.1	22.3	2.19	<LOD	18.4
18	18.1	24.4	<LOD	6.53	<LOD	2.72	2.0
19	1,109	218	2.23	685	<LOD	10.1	9.3
20	81.4	35.7	2.22	3.87	0.90	1.16	3.4
21	277	34.4	3.59	23.5	1.86	1.60	2.4
22	722	57.9	7.62	9.40	0.88	2.37	9.6

< LOD = Below level of detection.

biomarkers in oils derived from the Exshaw Fm. (Allan and Creaney, 1991). Further, accumulation of C_{org}-rich sediments in the Peace River Embayment has been previously connected to enhanced marine productivity in an upwelling zone (Caplan and Bustin, 1998; 2001). Previous geochemical analyses, however, focused on locations where the Exshaw Shale was most C_{org} rich, and our results expand this finding to show that sedimentary OM at all locations including those with relatively low C_{org} content has a marine origin.

The extent of bottom water anoxia during the deposition of Exshaw Shale at each location was assessed based on sedimentary facies classification and relative concentrations of trace elements. Trace fossil burrows in the Exshaw shale at Locs. 5, 15, 16, and 18 indicate greater oxygen exposure at the sediment surface during or soon after deposition on the Rundle Shelf adjacent to the Peace River Embayment and on the Madison Shelf adjacent to Prophet Trough (Visy, 2022). These locations also have elevated oxygen index values consistent with organic matter oxidation during early burial (Supplementary Table S1). Burrowing is interpreted to occur in shallower water environments where oxygenated conditions occur more frequently throughout the water column (Barclay et al., 1994; Richards et al., 1994; Smith et al., 1995; Smith and Bustin, 2000; Aretz and Corradini, 2021). Similarly, the TE enrichment factors were lowest at Locs. 3, 6, 8, 9, 16, 18, and 20, also indicating bottom waters in regions with burrows were more frequently oxygenated (Figures 3D, 5). While the entire basin was relatively shallow, the occurrence of subsidence by extensional faulting formed bathymetric lows that experienced more persistent stratification, thus those regions behaved as silled basins and were less prone to mixing between surface and bottom waters, similar to the modern Cariaco Basin (Thunell et al., 2004). Redox sensitive TE enrichment factors indicate that the deeper waters of the Peace River Embayment and Prophet Trough experienced oxygen depletion, whereas the paleobathymetric highs of the Rundle and Madison Shelf were comparatively oxygenated (Figure 5).

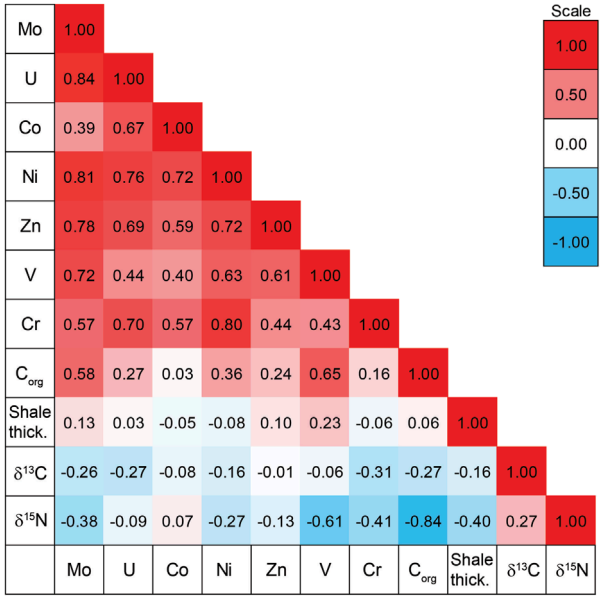

FIGURE 5
Spearman rank order correlation coefficients for trace element enrichment factors, organic carbon content (%), Exshaw Shale thickness (m), $\delta^{13}C_{org}$ (‰) and $\delta^{15}N_{tot}$ (‰).

4.2 Nutrient cycle

The nitrogen isotopic composition of marine sediments depends on the isotopic composition of phytoplankton and microbial transformations during transport to the ocean floor. Sinking particles are ^{15}N-enriched by ca. 0.15‰/200 m, so the N isotopic composition of sediments in shallow basins with anoxic bottom water broadly reflects average phytoplankton (Uveges et al., 2019). The inverse relationship between $\delta^{15}N$ and C_{org} at the base of the Exshaw Shale is intriguing (Figure 4), and the natural logarithmic fit ($R^2 = 0.83$) suggests the possible influence of Rayleigh fractionation of N isotopes during phytoplankton uptake (Okhouchi and Takano, 2014). The data can be explained by advection of surface waters from upwelling locations with high nutrient concentration, productivity, and OM accumulation to locations with low nutrient concentration, productivity, and OM accumulation. Thus, the low $\delta^{15}N$ values associated with higher sedimentary C_{org} would result from isotopic fractionation during incomplete assimilation of upwelled nutrients, leaving the residual nutrient pool ^{15}N-enriched. The higher $\delta^{15}N$ values associated with lower sedimentary C_{org} would derive from phytoplankton growth on the advected residual nutrient pool. The ^{15}N enrichment of the residual nutrient pool might also be affected by dissimilatory nitrification/denitrification and anammox, with the cumulative effect of assimilatory and dissimilatory processes contributing to the shape of the Rayleigh fractionation curve (Waser et al., 1998; Sigman et al., 2001; Altabet, 2005).

Collectively, phytoplankton populations preferentially draw on available NH_4^+ or NO_3 pools before N_2 fixation becomes widespread (Howarth et al., 1988). During oceanic anoxic events (OAEs), the global "Nitrostat" augments bioavailable N with increased N_2 fixation to replace N lost from the system due to increased denitrification and anammox (Kuypers et al., 2004). The concentrations of NH_4^+, NO_3^-, and NO_2^- (used as an electron acceptor in the anammox process) vary in the marine water column, depending on circulation, uptake by phytoplankton, ammonification during OM decomposition, and redox controls on microbial transformations (Sigman et al., 2001; Ohkouchi and Takano, 2014). In redox-stratified waters, nitrification, denitrification, and anammox are associated with the interface between reducing and oxidizing conditions and collectively diminish the nutrient-N pool. In deep waters below the photic zone, nutrient-N accumulates as NH_4^+ in anoxic waters and NO_3^- where O_2 ventilation supports nitrification (Junium et al., 2018). The anoxic/suboxic conditions that predominated in the WCSB favored bottom-water NH_4^+, which would constitute an internal N source that could support primary productivity when upwelled to the photic zone (Domingues et al., 2011; Peng, 2015; Naafs et al., 2019; Du et al., 2023).

In modern anoxic basins, the isotopic composition of bottom water NH_4^+ is similar to that of surface sediments. In the Cariaco Basin, deep NH_4^+ ($\delta^{15}N = 4.6‰$) is ^{15}N enriched by 1.2‰ compared with surface sediments ($\delta^{15}N$ = 3.4‰; Thunell et al., 2004). In the Black Sea, deep NH_4^+ ($\delta^{15}N$ = 1.7 ± 0.2‰; Velinsky et al., 1991) is ^{15}N depleted by ~1.2‰ compared with surface sediments ($\delta^{15}N$ = 2.9 ± 0.6‰; Fulton et al., 2012). Smaller stratified basins like Framvaren Fjord ($\delta^{15}N$ = 1.7‰ for deep NH_4^+ and 2.2‰ for surface sediments; Velinsky and Fogel, 1999) and Fayetteville Green Lake ($\delta^{15}N$ = 1.7‰ for deep NH_4^+ and 3.2‰ for surface sediments; Fulton et al., 2018) have similar relationships. The average isotopic difference ($\delta^{15}N_{NH4+}$ - $\delta^{15}N_{sed}$) for these four representative stratified anoxic basins is −0.5 ± 1.2‰, and we apply this value in the calculation of $\delta^{15}N$ of deep NH_4^+ for the WCSB during the onset of Exshaw Shale deposition. For 20 locations, the average $\delta^{15}N$ value for the base of the Exshaw Shale was 1.7‰ (weighted by C_{org} content). Therefore, the calculated average deep water $\delta^{15}N_{NH4+}$ value was 1.2 ± 1.2‰.

Unlike nutrient-N that can be fixed *in situ* from dissolved N_2, new phosphorus is mainly delivered to the ocean via continental weathering (Arthur and Sageman, 1994; Algeo and Scheckler, 2010). Sinking particulate matter transfers P along with N to deep waters and sediments. In the presence of O_2, N:P is typically close to the Redfield Ratio (16:1) for both particulate and dissolved components (Redfield, 1958; Falkowski et al., 1998; Tyrrell, 1999). In changing redox conditions, dissolved PO_4^{3-} concentration is regulated by adsorption and desorption from mineral phases (Furumai et al., 1989; Van Cappellen and Ingall, 1996; Ingalls et al., 2022). Under anoxic bottom waters, sedimentary P burial efficiency is reduced, leading to increased PO_4^{3-} concentration and decreased nutrient N:P, as has been observed in the Black Sea (Brewer and Murray, 1973; Fulton et al., 2012). Denitrification and anammox further contribute to lower N:P nutrient ratios. In such systems, upwelling of water with low N:P to the photic zone supports cyanobacterial N_2 fixation after nutrient-N has been exhausted.

For OAEs, modeled elevated PO_4^{3-} concentrations and enhanced denitrification contribute to elevated N_2 fixation. With a 2-fold increase in PO_4^{3-}concentration associated with OAE 2, the modeled global contribution to export includes 55% N_2 fixation, 35% NO_3^- assimilation, and 10% NH_4^+ assimilation (Naafs et al., 2019). Regions of high primary productivity were

focused in upwelling zones where NH_4^+ assimilation dominated, whereas N_2 fixation was prominent in locations receiving a low supply of bioavailable N. Martinez et al. (2019) reported ^{15}N-enrichment throughout the Cleveland Shale interval in the Appalachian Basin for the D-C boundary, which they associated with increased denitrification rates during a transgressive event. Other D-C boundary sections reported negative $\delta^{15}N$ excursions interpreted as indicative of increased N_2 fixation (Caplan and Bustin, 1998; Liu et al., 2016), following the common interpretation for similar ^{15}N-depleted black shales in Cretaceous marine sediments (Kuypers et al., 2004; Ohkouchi et al., 2006; Junium and Arthur, 2007; Monteiro et al., 2012; Fujisaki et al., 2016; Ruebsam and Schwark, 2023).We propose spatial variability in nutrient availability within the WCSB could drive the observed differences in the N isotopic composition of Exshaw Shale sediments (Figure 3). Similar variability in N cycling has also been proposed for the D-C boundary associated with complex paleogeography and location-specific differences in the extent of denitrification across a shallow marine basin in South China (Liu et al., 2016). We consider the role of surface water advection as the primary driver of divergent sedimentary $\delta^{15}N$ values.

4.3 Nutrient advection model

The variability of $\delta^{15}N$ within the WCSB (Figure 3), and its inverse relationship with C_{org} (Figure 4) may be most directly related to isotopic fractionation during incomplete assimilation of upwelled nutrients and subsequent surface water advection. This differs from the common interpretation that isotopic fractionation during denitrification and N_2 fixation is the direct cause of higher and lower $\delta^{15}N$ values, respectively. Kinetic isotopic fractionation is quantified by the isotope enrichment factor, denoted by epsilon (ε). For N, $^{15}\varepsilon$ reflects the ratio of the reaction rate constants (k) of light (^{14}N) and heavy (^{15}N) isotopes.

$$^{15}\boldsymbol{\varepsilon} = \left(^{14}\boldsymbol{k}/^{15}\boldsymbol{k} - \mathbf{1}\right) \times \mathbf{1000}(‰) \tag{1}$$

This calculation yields a positive $^{15}\varepsilon$ value for a normal kinetic isotope effect with ^{14}N reacting faster than ^{15}N. Isotopic fractionation between nutrient-N and biomass depends on the N source, which is affected by redox conditions. The $^{15}\varepsilon$ for NH_4^+ assimilation can vary widely from 4 to 27‰ depending on its concentration. In NH_4^+ replete conditions as would be expected for OAEs, partial uptake with $^{15}\varepsilon \geq 20‰$ can produce phytoplankton biomass with exceptionally low $\delta^{15}N$, leaving behind an exceptionally ^{15}N-enriched NH_4^+ pool (Waser et al., 1998; Higgins et al., 2012). The $^{15}\varepsilon$ value for NO_3^- assimilation in modern sea surface water is ~5‰ (Sigman et al., 1999).

The isotopic composition of phytoplankton biomass can be calculated by applying the Rayleigh equation for isotopic fractionation:

$$\boldsymbol{\delta}_{org} = \boldsymbol{\delta}_{init} + \mathbf{f}/(1-\mathbf{f}) \cdot \boldsymbol{\varepsilon} \cdot \ln(\mathbf{f}) \tag{2}$$

where δ_{org} is the $\delta^{15}N$ value for biomass N, δ_{init} is the $\delta^{15}N$ value for the nutrient source, $^{15}\varepsilon$ is the isotope enrichment factor, and f is the fraction of unutilized nutrient-N in the system after assimilation, i.e., the ratio of NH_4^+/NH_4^+-initial, and NO_3^-/NO_3^--initial. For high C_{org} ($\delta^{15}N$ = 6.0‰), moderate C_{org} ($\delta^{15}N$ = 2.4‰), and low C_{org} ($\delta^{15}N$ = 0.5‰) locations (Figure 4), we assessed the range of potential δ_{init} values as a function of residual nutrient-N ($0 \leq f \leq 1$) for $^{15}\varepsilon$ = 20‰ (a relatively conservative value for NH_4^+ assimilation, Figure 6A) and $^{15}\varepsilon$ = 5‰ (NO_3^- assimilation; Figure 6D).

Using Eq. 2 and isotope mass balance, $\delta^{15}N$ of the residual nutrient pool (δ_{resid}) as a function of δ_{init}, δ_{org}, and f is determined as follows:

$$\boldsymbol{\delta}_{resid} = \left[\boldsymbol{\delta}_{init} - (1-\mathbf{f}) \cdot \boldsymbol{\delta}_{org}\right]/\mathbf{f} \tag{3}$$

The δ_{resid} values increase dramatically with greater assimilation of the initial nutrient pool, resulting in $\delta^{15}N$ values much greater than any observed in the Exshaw sediments (Figures 6B,E). Assuming that the residual nutrient pool was advected away from the upwelling source and supported phytoplankton growth in less productive locations, the residual nutrient-N concentrations would decrease and the $\delta^{15}N$ would increase even more. However, if the initial upwelled nutrient pool had an N:P ratio lower than the Redfield ratio as expected for anoxic bottom waters, and PO_4^{3-} was advected in the surface waters along with nutrient-N, then the nutrient N:P ratio of advected waters would become progressively lower (assuming uptake close to the Redfield ratio). Thus, the advected water mass would have excess P that could ultimately support N_2 fixation distant from the initial upwelling region. Given the maximum $\delta^{15}N$ value near 6.0‰ for the base of the Exshaw Fm., cyanobacterial N_2 fixation in locations distal to upwelling would be required to lower the very high phytoplankton $\delta^{15}N$ values predicted for assimilation of advected nutrient-N (δ_{resid}).

The ratio of N_2 fixation to total N assimilation (r) can be defined as:

$$\mathbf{r} = \boldsymbol{\delta}_{resid} - \boldsymbol{\delta}_{org}/\boldsymbol{\delta}_{resid} - \boldsymbol{\delta}_{fix} \tag{4}$$

where $0 \leq r \leq 1$ and $\delta_{fix} = -1‰$ for N_2 fixation. (Modified from Eqs 2 and 3; Ohkouchi and Takano, 2014). The range of values for r required to produce observed δ_{org} values for the Exshaw Fm. are shown in Figures 6C,F.

We consider three example scenarios to evaluate nutrient utilization based on the advection model for the WCSB (Figure 7). All three scenarios feature deep NH_4^+ as the primary N-nutrient source in the WCSB and allow for N_2 fixation after NH_4^+ has been consumed.

1. Deep-water with $\delta^{15}N$-NH_4^+ = 1.2‰ is upwelled or mixed directly to the surface, where it is assimilated by phytoplankton. Residual NH_4^+ is advected away from the region of focused upwelling to less productive locations (Figure 7A).
2. Near the chemocline, NH_4^+ diffuses or slowly upwells from deep waters and is partially oxidized by anammox or nitrification/denitrification to N_2, leaving behind a ^{15}N-enriched NH_4^+ pool that supports phytoplankton growth above or at the top of the chemocline (Figure 7B).
3. Above the chemocline, upwelled NH_4^+ is nitrified, resulting in a NO_3^- pool with a $\delta^{15}N$ value that is lower than that of NH_4^+ at the chemocline, but more ^{15}N-enriched than deep-water NH_4^+ (Figure 7C).

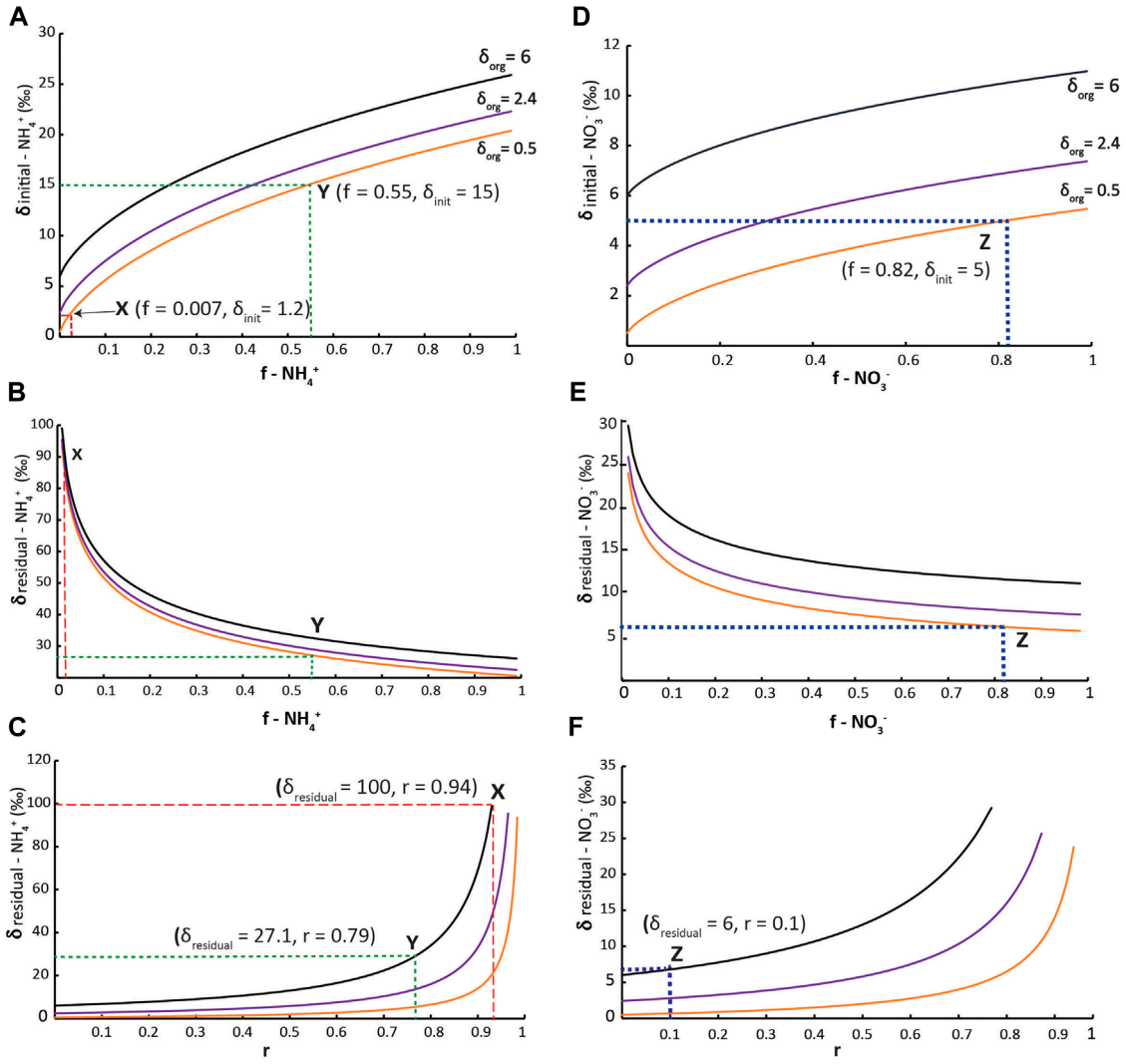

FIGURE 6
Upwelling and advection model. Panels **(A,D)** show the relationships between δ_{org}, δ_{init}, and f from Eq. 2 for $^{15}\varepsilon$ = 20‰ **(A)** and $^{15}\varepsilon$ = 5‰ **(D)**. Panels **(B,E)** show the distribution of δ_{resid} values for δ_{org} and f values from **(A,D)**, respectively, calculated by Eq. 3. Panels **(C,F)** show the ratios (r) of N_2 fixation to total N assimilation required to yield δ_{org} = 6.0, 2.4, and 0.5‰ for the δ_{resid} values in **(B,E)**, respectively. **(A–C)** (1) Point X shows ammonium replete conditions, upwelling and almost complete consumption resulting in very high residual isotope values. Point Y has a lower isotopic fractionation due to relatively higher $\delta^{15}N_{init}$ values, followed by advection of residual nutrient pool to N limited regions. N_2 fixation brings the very heavy residual ammonium to ambient values. **(D–F)** Point Z shows nitrate assimilation and advection of the residual nutrient pool.

With the three scenarios, we estimated the initial $\delta^{15}N$ values of nutrient-N that would support the production of biomass. We considered three characteristic locations in the WCSB with high (19.0% ± 0.8%), moderate (7.7% ± 2.6%), and low (0.8% ± 0.8%) C_{org} and average $\delta^{15}N$ values of 0.5‰, 2.4‰, and 6.0‰, respectively, based on Figure 4. Using the advection model parameters, our goal was to determine which scenario fits best with our observed $\delta^{15}N$ and C_{org} data and calculate a range of expected values for proportion of N fixation: assimilation (r). The lowest $\delta^{15}N$ values corresponded to productive upwelling locations with minimal N_2 fixation.

Scenario 1: Using the weighted average $\delta^{15}N_{sed}$ value of 1.7‰, the calculated $\delta^{15}N$ of deep water NH_4^+ in the WCSB is 1.2‰. In this scenario deep-water NH_4^+ is upwelled to the surface with minimal isotopic fractionation and supplied a nutrient-N source to phytoplankton with a low initial $\delta^{15}N$ value (Figure 7A). This scenario is analogous to the whole water-column mixing model of Uveges and Pearson (2023), which shows that low sedimentary $\delta^{15}N$ values are a result of periodic overturning of a stratified water column in an anoxic ocean. Assuming a high concentration of upwelled NH_4^+ was partially utilized, the resulting $^{15}\varepsilon$ would be high. The most productive locations with highest C_{org} would require f < 0.01 to produce δ_{org} = 0.5‰ with $\delta^{15}N_{init}$ = 1.2‰ and $^{15}\varepsilon$ = 20‰ (Point X in Figure 6A), implying near complete consumption of NH_4^+ at the site of upwelling. Thus, the advected residual NH_4^+ pool would be very small and ^{15}N-enriched (Point X in Figure 6B). To produce a maximum $\delta^{15}N_{sed}$ value of 6.0‰, phytoplankton production would require 94% of N to be derived from N_2 fixation (Point X in Figure 6C).

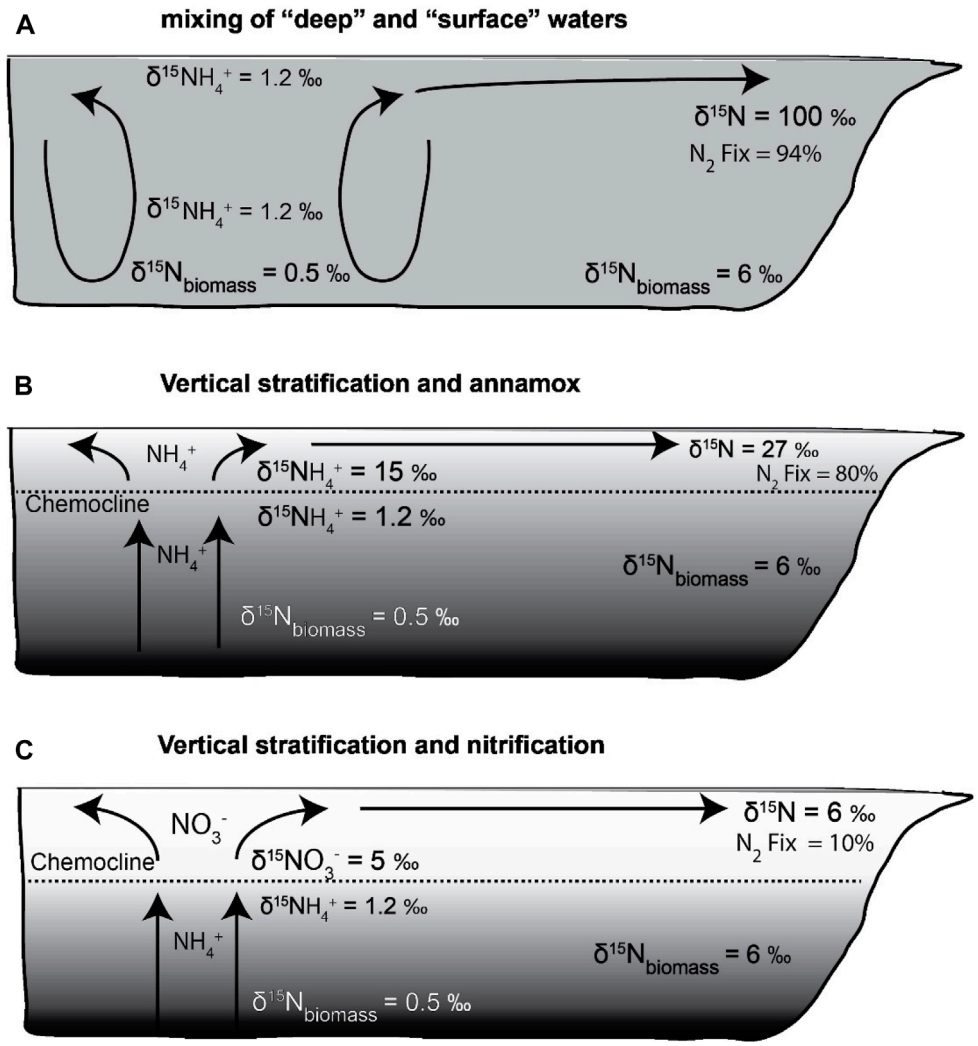

FIGURE 7
(A) Scenario 1: Low δ^{15}N- NH_4^+ rich deep waters were upwelled and mixed with surface waters. They are almost completely assimilated by phytoplankton, followed by advection of residual high δ^{15}N-NH_4^+ away from the region of upwelling. Distal locations experienced very high N_2 fixation to maintain productivity. **(B)** Scenario 2: Diffusion or gradual upwelling of NH_4^+ resulted in partial oxidation to N_2, leaving behind a ^{15}N-enriched NH_4^+ pool that supported phytoplankton growth near the chemocline. **(C)**: Scenario 3: Above the chemocline, upwelled NH_4^+ gets nitrified, resulting in a NO_3^- pool with a δ^{15}N value that is lower than that of NH_4^+ at the chemocline, but more ^{15}N-enriched than deep-water NH_4^+. Low N_2 fixation in distal areas as most of nutrient-N gets advected.

Scenario 2: In a strongly stratified basin that inhibits deep mixing, NH_4^+ diffuses to the chemocline and is utilized by annamox and nitrifying/denitrifying bacteria (Konovalov et al., 2008; Romaniello and Derry, 2010). This would increase the NH_4^+ δ^{15}N value of the residual pool. With strong stratification, the concentration of NH_4^+ decreases upward through the chemocline, and NH_4^+ δ^{15}N values can range up 10–20‰ at and above the chemocline (Fulton et al., 2018). In scenario 2, we assume a δ^{15}N value of 15‰ for NH_4^+ that is assimilated by phytoplankton at the top of the chemocline (Figure 7B). At the most productive locations with the highest C_{org}, this would require f = 0.55 to produce δ_{org} = 0.5‰ with $^{15}\varepsilon$ = 20‰ (Point Y in Figure 6A). The δ^{15}N value of the residual NH_4^+ pool would be predicted to be 27.1‰ (Point Y in Figure 6B). Using Eq. 4, complete assimilation of the residual NH_4^+ along with additional 79% N_2 fixation would account for δ_{resid} = 27.1‰ and δ_{org} = 6‰ (Point Y in Figure 6C). This means that the advected NH_4^+ residual pool would provide 21% of the N requirement in the most oligotrophic locations, and 79% N_2 fixation could make up for the N-deficit.

Scenario 3: During upward mixing of chemocline water, NH_4^+ might be nitrified and partially denitrified as it is mixed into oxygenated surface waters, thereby producing a NO_3^- pool with relatively high δ^{15}N (Figure 7C). We apply a value of 5‰, which is similar to observed surface water NO_3^- δ^{15}N values in modern oxygen-limited basins (Brandes et al., 1998; Voss et al., 2001). In the WCSB, with δ_{init} = 5‰, the most productive locations with highest C_{org} would require f = 0.18 (Point Z in Figure 6D), i.e., 82% of the initial NO_3^- would be transported away from the upwelling/mixing region by advection. Consequently, the advected nutrients could support greater primary productivity, as most of

the NO_3^- (82%) would be laterally advected. This could explain progressively higher phytoplankton $\delta^{15}N$ values away from the source region, but not decreasing C_{org}. This scenario does not permit the introduction of significant N_2 fixation with r = 0.10 (Point Z in Figure 6F); thus, there is not a mechanism to replace nutrient-N lost to denitrification/anammox near the chemocline.

The advection model investigates the spatial variability of nitrogen isotopic distributions in the WCSB, assuming NH_4^+ and NO_3^- as potential sources of bioavailable nitrogen in upwelling and stratified systems to account for a range of mixing scenarios. A component of N_2 fixation is present in all scenarios, but its extent varies with $\delta^{15}N_{initial}$ and uptake ε values. Scenarios 1 and 2 represent the two end members of NH_4^+ utilization by phytoplankton. The former depicts a scenario of mixing of surface and deep waters due to a "chemocline collapse" and therefore upwelled NH_4^+ is isotopically light, whereas the latter demonstrates a situation of vertical stratification that results in a ^{15}N-enriched NH_4^+pool being consumed by phytoplankton (Figures 7A,B). During stable periods, NH_4^+ accumulates under the chemocline. When this stratification breaks down, the NH_4^+gets released rapidly into the upper water layers. The third scenario holds true for modern OMZs, where the dissolved nitrogen pool is predominantly NO_3 formed by nitrification of NH_4^+ as it reaches the surface (Figure 7C). Models predicting nutrient utilization during OAEs record effects of both NH_4^+ and NO_3^- assimilation at different stages of redox stratification, contributing towards the final $\delta^{15}N$ of exported biomass (Naafs et al., 2019; Uveges and Pearson, 2023). In the WCSB, an upwelling zone within the Peace River Embayment supported assimilation of a ^{15}N depleted nutrient pool (NH_4^+). Portions of the Prophet Trough region and locations adjacent to the Sweetgrass Arch also have evidence for upwelled NH_4^+. Across the interior parts of the epicontinental basin, on the Rundle and Madison Shelf, higher sediment $\delta^{15}N$ values with low to moderate primary productivity suggest that N_2 fixation provided a greater portion of bioavailable nitrogen to sustain productivity. Without the influence of N fixation, the $\delta^{15}N$ values would be even higher in the low-productivity continental shelf regions.

At the six locations with stratigraphic profiles representing shallow shelf and deeper Prophet Trough and Peace River Embayment provinces, there was a general relationship between $\delta^{15}N$ values and C_{org} content (Figure 2). Low $\delta^{15}N$ values are recorded in association with C_{org} maxima at the base of the Exshaw and gradually increase across the lower shale and upper siltstone deposits. An overall positive shift of 4–6‰ in $\delta^{15}N$ is observed from the base of the Lower Shale to the contact between the upper siltstone and Banff Fm., possibly due to a redox switch from basin-wide anoxia during the onset of Exshaw deposition, to more oxygenated environments towards the upper Exshaw and Banff interval (Savoy, 1992). The End-Devonian OAE primarily sustained suboxic to anoxic conditions, based on TE data, and was probably more oxygenated relative to other major OAEs in the Phanerozoic. The decreasing TE enrichment up-core above the Exshaw Shale (Supplementary Figure S1) confirms more frequent oxygenation of bottom waters. Nitrogen isotope values, however, are primarily influenced by primary production, rather than by redox conditions as suggested by the strong correlation between $\delta^{15}N$ and C_{org} and weak correlation with redox-sensitive trace elements from the base of the Exshaw Shale (Figure 5). This suggests that preservation or post-depositional bottom-water redox conditions have relatively little impact on nitrogen isotope signals.

4.4 Carbon cycle

The range of $\delta^{13}C_{org}$ values at the base of the Exshaw Fm. (−26.8 to −29.5‰; Figure 4). indicates that the isotopic composition of OM was influenced by local factors in addition to the global atmospheric signature. A similar range of values was distributed stratigraphically through the Exshaw Fm., and $\delta^{13}C_{org}$ was not correlated strongly with C_{org} either spatially or stratigraphically (Figures 2, 5). This range of values for the D-C boundary interval has been reported globally, including in the English River Formation in southeastern Iowa (Heath et al., 2021); the Kronhofgraben section in the Carnic Alps and Rhenish Massif in Germany (Kaiser et al., 2006; Agnieszka et al., 2020; Hartenfels et al., 2022); the Holy Cross mountains in Poland (Marynowski and Filipiak, 2007; Malec, 2013; Matyja et al., 2021), and the Cat Ba Island in Vietnam (Komatsu et al., 2014; Paschall et al., 2019; Shizuya et al., 2020). At the initiation of the black shale deposition, a shift towards lower $\delta^{13}C_{org}$ values was observed in many D-C successions, including in the WCSB. Heath et al. (2021) reported an abrupt negative C_{org} isotope excursion at the onset of shale deposition, and a coincident increase in C_{org} content from the Burlington Shelf in southeastern Iowa. This is consistent with our sections at Loc. 9 and 11 on the Madison Shelf but not the deeper water locations in Prophet Trough, where $\delta^{13}C_{org}$ decreased gradually in the shale, or in the Peace River Embayment, where there was no C isotope excursion in the shale unit (Figure 2).

Broadly, $\delta^{13}C_{org}$ signals are a function of the isotopic composition of dissolved inorganic carbon (DIC), biological productivity, and growth temperatures. Local variations in the concentration and $\delta^{13}C$ of the source DIC are especially influential, as $\delta^{13}C_{org}$ values are sensitive to changes in the partitioning of ^{13}C and ^{12}C between organic carbon and carbonate (Velinsky and Fogel, 1999; Uveges et al., 2019). Microbially respired DIC that is ^{13}C-depeleted when upwelled in epicontinental margins and assimilated by primary producers can influence the isotopic composition of the exported OM, causing lower $\delta^{13}C_{org}$ values of marine sediment (Paschall et al., 2019; Pisarzowska et al., 2020). A broad trend of increasing carbonate $\delta^{13}C$ values across the D-C boundary has also been recognized in association with the Hangenberg event (Brand et al., 2004; Kaiser et al., 2006; Myrow et al., 2013; Kumpan et al., 2015; Martinez et al., 2019; Heath et al., 2021). It has been interpreted as a global signal resulting from increased burial of ^{13}C-depleted C_{org} and concomitant ^{13}C enrichment of residual CO_2 in the atmosphere and DIC in the ocean (Buggisch and Joachimski, 2006; Bojar et al., 2013; Qie et al., 2016; Heath et al., 2021).

Lithologic variability within the Exshaw-Banff succession records variability in sea level during the D-C transition. An initial episode of transgression coincided with deposition of the C_{org}-rich Lower Shale of the Exshaw and a subsequent sea level fall and deposition of the upper siltstone (Macqueen and Sandberg, 1970). The siltstone unit was in turn followed by a second episode of transgression, and deposition of the calcareous Banff Shale. (Savoy, 1992; Robison, 1995; Figure 3, Supplementary Figure S4). This lithological sequence can potentially affect the occurrence

of C isotope excursions associated with the Hangenberg event and/or the D-C boundary. In the WCSB, the D-C boundary occurs within the Exshaw Fm. (Caplan and Bustin, 1998). However, given the complex bathymetry of the WCSB, eustatic sea level change, and active tectonism at the time of deposition, it might not be definitively in the same lithologic unit at all locations. For example, at Loc. 21 and 22, the positive C isotope excursion appears to coincide with the Lower Shale/Upper Shale transition (Figure 2). At Loc. 11, there is a similar excursion at the Exshaw shale/siltstone transition. At Loc. 4, 9, and 11 there is a $\delta^{13}C_{org}$ increase at the Exshaw/Banff boundary (Figure 2). The C_{org} content in all six locations with stratigraphic profiles record a decreasing trend within the Exshaw to the Banff succession (Figure 2). Carbon isotope values are generally stable in the shale or Lower Shale intervals; however, a shift to higher values and a correlative decrease in C_{org} is observed across the Exshaw-Banff boundary (Figure 2). A paleoclimatic shift from a greenhouse to icehouse climate may have been responsible for the observed trend in $\delta^{13}C_{org}$ across the Exshaw-Banff boundary, since perturbations in the global carbon cycle are primarily related to atmospheric CO_2 levels (Becker et al., 2016a; Tuite et al., 2019; Zhang et al., 2021).

4.5 Relationship to modern coastal eutrophication

Nutrient cycling in past oceans might be analogous to the future, offering clues about how ocean ecosystems respond to shifts in nutrient availability. Environmental forcings that are currently causing coastal eutrophication and formation of oxygen minimum zones in modern oceans are mechanistically similar to forcings associated with some of the major marine biotic disruptions in the past (Paulmier and Ruiz-Pino, 2009; Zhou et al., 2016). The Devonian OAE was connected with the evolution of land plants and their extended root systems penetrating into the soil and amplifying the rates of continental weathering (Algeo and Scheckler, 2010). Consequently, there was an increase in the nutrient flux to the epicontinental seas, and globally widespread anoxia ensued. In modern oceans, warmer temperatures have intensified ocean stratification, which coupled with anthropogenic nutrient discharge in shallow seas has resulted in local stimulation of primary productivity and impinging coastal anoxia in many major continental margins and some restricted basins as well (De Pol-Holz et al., 2009; Domingues et al., 2011; Elfi Mollier-Vogel et al., 2012; Fulton et al., 2012; Brandt et al., 2023). Since continental margins are hotspots for marine biodiversity, prediction of nutrient circulation and transport pathways can help identify areas of the modern ocean that are particularly sensitive to nutrient imbalances. From this study we infer that high primary productivity is spatially tied to upwelling zones, with minimal local requirement for N_2 fixation. As with modern upwelling zones, the primary producers were likely eukaryotic algae. The parts of the basin distant from upwelling were more oligotrophic and required a greater contribution of N_2 fixation by cyanobacteria to balance the "nitrostat".

Nitrogen isotope gradients in modern low oxygen environments like the western coasts of Peru and Ecuador suggest that advection patterns in nutrient utilization are characteristic of upwelling systems. The subsurface waters of the Eastern South Pacific coast host intensified OMZs due to high primary productivity and slow ventilation. As upwelling intensity varies spatially across the continental margin, it is reflected in sedimentary N isotope gradients that can be traced to different degrees of oxygen limitation (Elfi Mollier-Vogel et al., 2012). The Chilean margin also documents a strong latitudinal variability in sedimentary $\delta^{15}N$ values, due to the lateral transport of ^{15}N-enriched waters from an upwelling zone in the south of the OMZ towards higher latitudes (De Pol-Holz et al., 2009). The N-dynamics from modern upwelling zones confirm our interpretations of nutrient circulation across the D-C boundary in the WCSB. This phenomenon is not confined to the Devonian period alone, as anoxic oceans were prevalent throughout Earth's history, and similar marine transgressive events have played a role consistently in facilitating the development of stratification and anoxia (Arthur and Sageman, 2004). Our interpretations of the influences of advection and upwelling on nitrogen isotopes in various depositional settings are not only applicable to past anoxic events but also enhance our understanding of nutrient circulation patterns in modern oxygen minimum zones. This knowledge is crucial for predicting how current and future changes in oceanographic conditions might impact marine ecosystems, particularly in regions susceptible to low oxygen levels. By integrating spatial variations in nitrogen fixation rates with nutrient transport and utilization models, we could potentially predict niche partitioning of eukaryotic algae versus cyanobacterial communities, allowing for a more comprehensive understanding of the interplay between nutrient availability and marine productivity patterns.

5 Conclusion

The Devonian-Carboniferous transition was a period of widespread deoxygenation in the oceans, associated with the Hangenberg mass extinction event that led to large-scale evolutionary transformations in the marine ecosystem. Temporal and spatial isotopic and C_{org} variability were observed in black shales deposited during the Hangenberg OAE in the Western Canada Sedimentary Basin.

The degree of anoxia varied across the WCSB between the deep embayment and shallower cratonic shelf, due to proximity to the upwelling zone. This resulted in local differences in nutrient-N availability and a disparity in the balance between NH_4^+ assimilation and N fixation rates. Spatial variability of bioavailable N across an anoxic shallow marine basin generated large differences in the distribution of primary productivity, which is evident from sedimentary $\delta^{15}N$ records. A negative excursion in $\delta^{15}N$ at the base of the Exshaw Fm. corresponding to a C_{org} maximum indicates high primary productivity was connected to decreased $\delta^{15}N$ values. Up-core, increasing $\delta^{15}N$ values were associated with lower productivity in surface waters. Carbon isotopic compositions, however, are relatively consistent at the D-C boundary across the basin and comparable to other D-C black shale successions globally.

Our model depicts nutrient utilization and advection scenarios across different productivity regimes. Using a modified Rayleigh isotopic fractionation equation, the $\delta^{15}N$ value of the initial nutrient-N pool consumed by phytoplankton is determined from the observed $\delta^{15}N$ values, and the corresponding amounts of N_2 fixation predicted for both high and low-productivity areas. Through this

study, it can be inferred that during the End-Devonian OAE, Western Canada experienced anoxic conditions across the basin with NH_4^+ as the predominant bioavailable source of nitrogen, and periodic collapse of stratification resulted in mixing of surface and deep waters. The effects of NH_4^+ and NO_3^- assimilation at different stages of redox stratification contributed to final $\delta^{15}N$ values of exported biomass.

Data availability statement

The original contributions presented in the study are publicly available. This data can be found in the Texas Data Repository: hhttps://doi.org/10.18738/T8/NAA3M9

Author contributions

SD: Conceptualization, Data curation, Formal Analysis, Investigation, Methodology, Software, Writing–original draft, Writing–review and editing. MF: Data curation, Investigation, Methodology, Validation, Writing–review and editing. SA Funding acquisition, Investigation, Project administration, Resources, Supervision, Validation, Writing–review and editing. JF: Conceptualization, Funding acquisition, Investigation, Methodology, Project administration, Resources, Supervision, Validation, Visualization, Writing–original draft, Writing–review and editing.

Funding

The author(s) declare financial support was received for the research, authorship, and/or publication of this article. Financial support for this research and publication was provided by Baylor University Faculty Development fund and Baylor University Applied Petroleum Studies program.

Acknowledgments

We acknowledge the Alberta Energy Regulator Core Research Centre for access to core material. We thank Ren Zhang of the Baylor Stable Isotope Lab for C and N isotope analyses. Julia Visy (Baylor Department of Geosciences) assisted in sample collection and core descriptions and Jillian Sturtevant (Baylor Department of Environmental Science) contributed to spatial correlations using ArcGIS. Christopher K. Junium from Syracuse University provided helpful feedback on an earlier draft of the manuscript, and comments from three reviewers improved the final version.

Conflict of interest

The authors declare that the research was conducted in the absence of any commercial or financial relationships that could be construed as a potential conflict of interest.

Supplementary material

The Supplementary Material for this article can be found online at: https://www.frontiersin.org/articles/10.3389/feart.2024.1407639/full#supplementary-material

References

Agnieszka, P., Michał, R., Leszek, M., Marek, S., Marie, T., Mariusz, P., et al. (2020). Large environmental disturbances caused by magmatic activity during the Late Devonian Hangenberg Crisis. *Glob. Planet. Change* 190, 103155. doi:10.1016/j.gloplacha.2020.103155

Algeo, T. J., and Li, C. (2020). Redox classification and calibration of redox thresholds in sedimentary systems. *Geochim. Cosmochim. Acta.* 287, 8–26. doi:10.1016/j.gca.2020.01.055

Algeo, T. J., and Liu, J. (2020). A re-assessment of elemental proxies for paleoredox analysis. *Chem. Geol.* 540, 119549. doi:10.1016/j.chemgeo.2020.119549

Algeo, T. J., and Scheckler, S. E. (2010). Land plant evolution and weathering rate changes in the Devonian. *J. Earth Sci.* 21 (1), 75–78. doi:10.1007/s12583-010-0173-2

Algeo, T. J., and Tribovillard, N. (2009). Environmental analysis of paleoceanographic systems based on molybdenum–uranium covariation. *Chem. Geol.* 268 (3-4), 211–225. doi:10.1016/j.chemgeo.2009.09.001

Allan, J., and Creaney, S. (1991). Oil families of the western Canada basin. *Bull. Can. Pet. Geol.* 39 (2), 107–122. doi:10.35767/gscpgbull.39.2.107

Altabet, M. A. (2005). Isotopic tracers of the marine nitrogen cycle: present and past. *Hdb Env. Chem.* 2, 251–293. doi:10.1007/698_2_008

Altabet, M. A., Higginson, M. J., and Murray, D. W. (2002). The effect of millennial-scale changes in Arabian Sea denitrification on atmospheric CO_2. *Nat. Geosci.* 415, 159–162. doi:10.1038/415159a

Aretz, M., and Corradini, C. (2021). Global review of the Devonian-Carbonifereous boundary: an introduction. *Palaeobiodiv. Palaeoenv.* 101 (2), 285–293. doi:10.1007/s12549-021-00499-8

Arthur, M. A., and Sageman, B. B. (1994). Marine black shales: depositional mechanisms and environments of ancient deposits. *Annu. Rev. Earth Planet. Sci.* 22 (1), 499–551. doi:10.1146/annurev.ea.22.050194.002435

Arthur, M. A., and Sageman, B. B. (2004). *Sea-Level control on source-rock development: perspectives from the Holocene Black Sea, the Mid-Cretaceous western interior basin of north America, snd the Late Devonian Appalachian Basin.* SEPM (Society for Sedimetary Geology, 35–59. ISBN 1-56576-110-3.

Bábek, O., Kumpan, T., Kalvoda, J., and Matys Grygar, T. (2016). Devonian/Carboniferous boundary glacioeustatic fluctuations in a platform-to-basin direction: a geochemical approach of sequence stratigraphy in pelagic settings. *Sediment. Geol.* 337, 81–99. doi:10.1016/j.sedgeo.2016.03.009

Barclay, J., Richards, B. C., Bryant, D., Henderson, C., Hartling, A., and Trollope, F. (1994). *Carboniferous strata of the western Canada sedimentary Basin* in geological atlas of the western Canada. Chapter 14.

Becker, R. T., Kaiser, S. I., and Aretz, M. (2016b). Review of chrono, litho and biostratigraphy across the global Hangenberg crisis and Devonian–Carboniferous boundary. *Geol. Soc. Lond. Spec. Pub.* 423 (1), 355–386. doi:10.1144/sp423.10

Becker, R. T., Königshof, P., and Brett, C. E. (2016a). Devonian climate, sea level and evolutionary events: an introduction. *Geol. Soc. Lond. Spec. Pub.* 423 (1), 1–10. doi:10.1144/SP423.15

Blakey, R. (2008). Gondwana paleogeography from assembly to breakup—a 500 m.y. odyssey. *Geol. Soc. Am. Special Pap.* 441, 1–28. doi:10.1130/2008.2441(01

Bojar, A. V., Neubauer, F., and Koeberl, C. (2013). Geochemical record of Late Devonian to Early Carboniferous events, Palaeozoic of graz, eastern Alps, Austria. *Geol. Soc. Lond. Spec. Pub* 376 (1), 87–108. doi:10.1144/SP376.15

Brand, U., Legrand-Blain, M., and Streel, M. (2004). Biochemostratigraphy of the Devonian– Carboniferous boundary global stratotype section and point, Griotte Formation, La serre, montagne noire, France. *Palaeogeogr. Palaeoclimatol. Palaeoecol.* 205 (3-4), 337–357. doi:10.1016/j.palaeo.2003.12.015

Brandes, J. A., Devol, A. H., Yoshinari, T., Jayakumar, D. A., and Naqvi, S. W. A. (1998). Isotopic composition of nitrate in the Central Arabian Sea and eastern tropical North Pacific: a tracer for mixing and nitrogen cycles. *Limnol. Oceanogr.* 43 (7), 1680–1689. doi:10.4319/lo.1998.43.7.1680

Brandt, P., Alory, G., Awo, F. M., Dengler, M., Djakouré, S., Imbol Koungue, R. A., et al. (2023). Physical processes and biological productivity in the upwelling regions of the tropical Atlantic. *Ocean. Sci.* 19 (3), 581–601. doi:10.5194/os-19-581-2023

Brewer, P. G., and Murray, J. W. (1973). Carbon, nitrogen, and phosphorus in the Black Sea. *Deep-Sea Res. Oceanogr. Abstr.* 20 (9), 803–818. doi:10.1016/0011-7471(73)90003-x

Buggisch, W., and Joachimski, M. M. (2006). Carbon isotope stratigraphy of the Devonian of central and southern Europe. *Palaeogeogr. Palaeoclimatol. Palaeoecol.* 240 (1), 68–88. doi:10.1016/j.palaeo.2006.03.046

Calvert, S. E., Bustin, R. M., and Ingall, E. D. (1996). Influence of water column anoxia and sediment supply on the burial and preservation of organic carbon in marine shales. *Geochim. Cosmochim. Acta* 60 (9), 1577–1593. doi:10.1016/0016-7037(96)00041-5

Caplan, M. L., and Bustin, R. M. (1998). Palaeoceanographic controls on geochemical characteristics of organic-rich Exshaw mudrocks: role of enhanced primary production. *Org. Geochem.* 30 (2-3), 161–188. doi:10.1016/s0146-6380(98)00202-2

Caplan, M. L., and Bustin, R. M. (1999). Devonian–Carboniferous Hangenberg mass extinction event, widespread organic-rich mudrock and anoxia: causes and consequences. *Palaeogeogr. Palaeoclimatol. Palaeoecol.* 148 (4), 187–207. doi:10.1016/s0031-0182(98)00218-1

Caplan, M. L., and Bustin, R. M. (2001). Palaeoenvironmental and palaeoceanographic controls on black, laminated mudrock deposition: example from Devonian–Carboniferous strata, Alberta, Canada. *Sediment. Geol.* 145 (1-2), 45–72. doi:10.1016/s0037-0738(01)00116-6

Carbonel, C., and Valentin, J. L. (1999). Numerical modelling of phytoplankton bloom in the upwelling ecosystem of Cabo Frio (Brazil). *Ecol. Model.* 116 (2), 135–148. doi:10.1016/S0304-3800(98)00201-4

Dalsgaard, T., Thamdrup, B., Farías, L., and Revsbech, N. P. (2012). Anammox and denitrification in the oxygen minimum zone of the eastern South Pacific. *Limnol. Oceanogr.* 57 (5), 1331–1346. doi:10.4319/lo.2012.57.5.1331

De Pol-Holz, R., Robinson, R., Hebbeln, D., Sigman, D., and Ulloa, O. (2009). Controls on sedimentary nitrogen isotopes along the Chile margin. *Deep-Sea Res. II Top. Stud. Oceanogr.* 56, 1042–1054. doi:10.1016/j.dsr2.2008.09.014

Dhar, S. (2024). Bulk geochemical data of black shales in Western Canada: End-Devonian Period. *Tex. Data Repos.* V1. doi:10.18738/T8/NAA3M9

Domingues, R. B., Barbosa, A. B., Sommer, U., and Galvão, H. M. (2011). Ammonium, nitrate and phytoplankton interactions in a freshwater tidal estuarine zone: potential effects of cultural eutrophication. *Aquat. Sci.* 73, 331–343. doi:10.1007/s00027-011-0180-0

Du, Y., Song, H., Grasby, S. E., Xing, T., Song, H., Tian, L., et al. (2023). Recovery from persistent nutrient-N limitation following the Permian–Triassic mass extinction. *Earth Planet. Sci. Lett.* 602, 117944. doi:10.1016/j.epsl.2022.117944

Elfi Mollier-Vogel, E. R., Philippe, M., Wallace, D., Altabet, M. A., Schneider, R., and Schneider, R. (2012). Nitrogen isotope gradients off Peru and Ecuador related to upwelling, productivity, nutrient uptake and oxygen deficiency. *Deep-Sea Res.* 1, 14–25. doi:10.1016/j.dsr.2012.06.003

Falkowski, P. G., Barber, R. T., and Smetacek, V. (1998). Biogeochemical controls and feedbacks on ocean primary production. *Science* 281 (5374), 200–206. doi:10.1126/science.281.5374.200

Frucci, M. (2021). *Regional elemental and organic geochemical character of the devonian/mississippian Exshaw Formation across Alberta*. Canada: Baylor University. [Master's Thesis].

Fujisaki, W., Sawaki, Y., Yamamoto, S., Sato, T., Nishizawa, M., Windley, B. F., et al. (2016). Tracking the redox history and nitrogen cycle in the pelagic Panthalassic deep ocean in the Middle Triassic to Early Jurassic: insights from redox-sensitive elements and nitrogen isotopes. *Palaeogeogr. Palaeoclimatol. Palaeoecol.* 449, 397–420. doi:10.1016/j.palaeo.2016.01.039

Fulton, J. M., Arthur, M. A., and Freeman, K. H. (2012). Black Sea nitrogen cycling and the preservation of phytoplankton $\delta^{15}N$ signals during the Holocene. *Glob. Biogeochem. Cycles* 26 (2). doi:10.1029/2011GB004196

Fulton, J. M., Arthur, M. A., Thomas, B., and Freeman, K. H. (2018). Pigment carbon and nitrogen isotopic signatures in euxinic basins. *Geobiology* 16 (4), 429–445. doi:10.1111/gbi.12285

Furumai, H., Kondo, T., and Ohgaki, S. (1989). Phosphorus exchange kinetics and exchangeable phosphorus forms in sediments. *Water Res.* 23 (6), 685–691. doi:10.1016/0043-1354(89)90200-5

Hartenfels, S., Becker, R. T., Herbig, H.-G., Qie, W., Kumpan, T., De Vleeschouwer, D., et al. (2022). The Devonian-Carboniferous transition at Borkewehr near Wocklum (northern Rhenish Massif, Germany) – a potential GSSP section. *Palaeobio. Palaeoenv* 102 (3), 763–829. doi:10.1007/s12549-022-00531-5

Heath, M. H., Bradley, D. C., Brittany, M. S., Gwen, L. B., Ryan, J. C., James, E. D., et al. (2021). Chemoautotrophy as the driver of decoupled organic and carbonate carbon isotope records at the onset of the Hangenberg (Devonian-Carboniferous Boundary) Oceanic Anoxic Event. *Palaeogeogr. Palaeoclimatol. Palaeoecol.* 577, 110540. doi:10.1016/j.palaeo.2021.110540

Higgins, M. B., Robinson, R. S., Husson, J. M., Carter, S. J., and Pearson, A. (2012). Dominant eukaryotic export production during ocean anoxic events reflects the importance of recycled NH_4^+. *Proc. Nat. Acad. Sci.* 109 (7), 2269–2274. doi:10.1073/pnas.1104313109

Howarth, R. W., Marino, R., and Cole, J. J. (1988). Nitrogen fixation in freshwater, estuarine, and marine ecosystems. 2. Biogeochemical controls1. *Limnol. Oceanogr.* 33 (4part2), 688–701. doi:10.4319/lo.1988.33.4part2.0688

Ingalls, M., Grotzinger, J. P., Present, T., Rasmussen, B., and Fischer, W. W. (2022). Carbonate-associated phosphate (CAP) indicates elevated phosphate availability in neoarchean shallow marine environments. *Geophys. Res. Lett.* 49 (6), e2022GL098100. doi:10.1029/2022GL098100

Jenkyns, H. C. (2010). Geochemistry of oceanic anoxic events. *Geochem. Geophys. Geosys.* 11 (3). doi:10.1029/2009GC002788

Jewell, P. W. (1994). Paleoredox conditions and the origin of bedded barites along the Late Devonian north American continental margin. *J. Geol.* 102 (2), 151–164. doi:10.1086/629660

Junium, C. K., and Arthur, M. A. (2007). Nitrogen cycling during the Cretaceous, Cenomanian-Turonian oceanic anoxic event II. *Geochem. Geophys. Geosys.* 8(3). doi:10.1029/2006GC001328

Junium, C. K., Dickson, A. J., and Uveges, B. T. (2018). Perturbation to the nitrogen cycle during rapid Early Eocene global warming. *Nat. Comm.* 9 (1), 3186. doi:10.1038/s41467-018-05486-w

Kabanov, P., and Jiang, C. (2020). Photic-zone euxinia and anoxic events in a Middle-Late Devonian shelfal sea of Panthalassan continental margin, NW Canada: changing paradigm of Devonian ocean and sea level fluctuations. *Glob. Planet. Change* 188, 103153. doi:10.1016/j.gloplacha.2020.103153

Kaiser, S. I. (2005). Mass extinctions, climatic and oceanographic changes at the Devonian/Carboniferous boundary. Available at: http://www-brs.ub.ruhr-uni-bochum.de/netahtml/HSS/Diss/KaiserSandraIsabella/diss.pdf.

Kaiser, S. I., Aretz, M., and Becker, R. T. (2016). The global Hangenberg Crisis (Devonian–Carboniferous transition): review of a first-order mass extinction. *Geol. Soc. Lond. Spec. Pub.* 423 (1), 387–437. doi:10.1144/sp423.9

Kaiser, S. I., Steuber, T., Becker, R. T., and Joachimski, M. M. (2006). Geochemical evidence for major environmental change at the Devonian–Carboniferous boundary in the carnic Alps and the Rhenish Massif. *Palaeogeogr. Palaeoclimatol. Palaeoecol.* 240 (1-2), 146–160. doi:10.1016/j.palaeo.2006.03.048

Kämpf, J. (2016). On the majestic seasonal upwelling system of the Arafura Sea. *J. Geophys. Res. Oceans* 121 (2), 1218–1228. doi:10.1002/2015JC011197

Karstensen, J., Stramma, L., and Visbeck, M. (2008). Oxygen minimum zones in the eastern tropical Atlantic and Pacific oceans. *Prog. Oceanogr.* 77 (4), 331–350. doi:10.1016/j.pocean.2007.05.009

Kienast, S. S., Calvert, S. E., and Pedersen, T. F. (2002). Nitrogen isotope and productivity variations along the northeast Pacific margin over the last 120 kyr: surface and subsurface paleoceanography. *Paleoceanogr* 17 (1055). doi:10.1029/2001PA000650

Komatsu, T., Kato, S., Hirata, K., Takashima, R., Ogata, Y., Oba, M., et al. (2014). Devonian-Carboniferous transition containing a Hangenberg black shale equivalent in the Pho Han Formation on Cat Ba Island, northeastern Vietnam. *Palaeogeogr. Palaeoclimatol. Palaeoecol.* 404, 30–43. doi:10.1016/j.palaeo.2014.03.021

Konovalov, S. K., Fuchsman, C. A., Belokopitov, V., and Murray, J. W. (2008). Modeling the distribution of nitrogen species and isotopes in the water column of the Black Sea. *Mar. Chem.* 111, 106–124. doi:10.1016/j.marchem.2008.01.006

Kumar, S. P., Madhupratap, M., Dileepkumar, M., Muraleedharan, P. M., Souza, S. N., Gauns, M., et al. (2001). High biological productivity in the central Arabian Sea during the summer monsoon driven by Ekman pumping and lateral advection. *Curr. Sci.* 81, 1633–1638.

Kumpan, T., Bábek, O., Kalvoda, J., Grygar, T., Fryda, J., Becker, T. R., et al. (2015). Petrophysical and geochemical signature of the Hangenberg events: an integrated stratigraphy of the Devonian-Carboniferous boundary interval in the northern Rhenish Massif (Avalonia, Germany). *Bull. Geosci.* 90 (3), 667–694. doi:10.3140/bull.geosci.1547

Kuypers, M. M. M., Marchant, H. K., and Kartal, B. (2018). The microbial nitrogen-cycling network. *Nat. Rev. Microbio.* 16 (5), 263–276. doi:10.1038/nrmicro.2018.9

Kuypers, M. M. M., van Breugel, Y., Schouten, S., Erba, E., and Damsté, J. S. S. (2004). N_2-fixing cyanobacteria supplied nutrient N for Cretaceous oceanic anoxic events. *Geology* 32 (10), 853–856. doi:10.1130/G20458.1

Liu, J., Qie, W., Algeo, T. J., Yao, L., Huang, J., and Luo, G. (2016). Changes in marine nitrogen fixation and denitrification rates during the End-Devonian mass extinction. *Palaeogeogr. Palaeoclimatol. Palaeoecol.* 448, 195–206. doi:10.1016/j.palaeo.2015.10.022

Macqueen, R. W., and Sandberg, C. A. (1970). Stratigraphy, age, and interregional correlation of the Exshaw Formation, Alberta rocky mountains. *Bull. Can. Pet. Geol.* 18, 32–66. doi:10.35767/gscpgbull.18.1.032

Malec, J. (2013). The Devonian/Carboniferous boundary in the holy Cross mountains (Poland). *Geol. Qtly.* 58 (2). doi:10.7306/gq.1142

Martinez, A. M., Boyer, D. L., Droser, M. L., Barrie, C., and Love, G. D. (2019). A stable and productive marine microbial community was sustained through the End-Devonian Hangenberg Crisis within the Cleveland Shale of the Appalachian Basin, United States. *Geobiology* 17 (1), 27–42. doi:10.1111/gbi.12314

Marynowski, L., and Filipiak, P. (2007). Water column euxinia and wildfire evidence during deposition of the Upper Famennian Hangenberg event horizon from the Holy Cross Mountains (central Poland). *Geol. Mag.* 144 (3), 569–595. doi:10.1017/S0016756807003317

Marynowski, L., Zatoń, M., Rakociński, M., Filipiak, P., Kurkiewicz, S., and Pearce, T. J. (2012). Deciphering the upper Famennian Hangenberg Black Shale depositional environments based on multi-proxy record. *Palaeogeogr. Palaeoclimatol. Palaeoecol.* 346, 66–86. doi:10.1016/j.palaeo.2012.05.020

Matyja, H., Woroncowa-Marcinowska, T., Filipiak, P., Brański, P., and Sobień, K. (2021). The Devonian/Carboniferous boundary interval in Poland: multidisciplinary studies in pelagic (Holy Cross Mountains and Sudetes) and ramp (Western Pomerania) successions. *Palaeobio. Palaeoenv.* 101 (2), 421–472. doi:10.1007/s12549-020-00442-3

Monteiro, F. M., Pancost, R. D., Ridgwell, A., and Donnadieu, Y. (2012). Nutrients as the dominant control on the spread of anoxia and euxinia across the Cenomanian-Turonian oceanic anoxic event (OAE2): model-data comparison. *Paleoceanogr* 27 (4). doi:10.1029/2012PA002351

Murphy, A. E., Sageman, B. B., Hollander, D. J., Lyons, T. W., and Brett, C. E. (2000). Black shale deposition and faunal overturn in the Devonian Appalachian Basin: clastic starvation, seasonal water-column mixing, and efficient biolimiting nutrient recycling. *Paleoceanogr* 15 (3), 280–291. doi:10.1029/1999PA000445

Myrow, P., Strauss, J., Creveling, J., Sicard, K., Ripperdan, R., Sandberg, C., et al. (2011). A carbon isotopic and sedimentological record of the latest Devonian (Famennian) from the Western U.S. and Germany. *Palaeogeogr. Palaeoclimatol. Palaeoecol.* 306, 147–159. doi:10.1016/j.palaeo.2011.04.013

Myrow, P. M., Hanson, A., Phelps, A. S., Creveling, J. R., Strauss, J. V., Fike, D. A., et al. (2013). Latest Devonian (Famennian) global events in western Laurentia: variations in the carbon isotopic record linked to diagenetic alteration below regionally extensive unconformities. *Palaeogeogr. Palaeoclimatol. Palaeoecol.* 386, 194–209. doi:10.1016/j.palaeo.2013.05.021

Naafs, B. D. A., Monteiro, F. M., Pearson, A., Higgins, M. B., Pancost, R. D., and Ridgwell, A. (2019). Fundamentally different global marine nitrogen cycling in response to severe ocean deoxygenation. *Proc. Nat. Acad. Sci.* 116 (50), 24979–24984. doi:10.1073/pnas.1905553116

O'Connell, S. C., Dix, G., and Barclay, J. (1990). The origin, history, and regional structural development of the Peace River Arch, western Canada. *Bull. Can. Pet. Geo.* 38, 4–24. doi:10.35767/gscpgbull.38a.1.004

Ohkouchi, N., Kashiyama, Y., Kuroda, J., Ogawa, N., and Kitazato, H. (2006). The importance of diazotrophic cyanobacteria as primary producers during Cretaceous Oceanic Anoxic Event 2. *Biogeosc* 3, 467–478. doi:10.5194/bg-3-467-2006

Ohkouchi, N., and Takano, Y. (2014). "12.10 - organic nitrogen: sources, fates, and chemistry," in *Treatise on geochemistry*. Editors H. D. Holland, and K. K. Turekian Second Edition, 251–289.

Pajares, S., and Ramos, R. (2019). Processes and microorganisms involved in the marine nitrogen cycle: knowledge and gaps. *Front. Mar. Sci.* 6. doi:10.3389/fmars.2019.00739

Parrish, J. T. (1982). Upwelling and petroleum source beds, with reference to Paleozoic. *AAPG Bull.* 66 (6), 750–774. doi:10.1306/03b5a30e-16d1-11d7-8645000102c1865d

Paschall, O., Carmichael, S. K., Königshof, P., Waters, J. A., Ta, P. H., Komatsu, T., et al. (2019). The Devonian-Carboniferous boundary in Vietnam: sustained ocean anoxia with a volcanic trigger for the Hangenberg Crisis? *Glob. Planet. Change* 175, 64–81. doi:10.1016/j.gloplacha.2019.01.021

Paulmier, A., and Ruiz-Pino, D. (2009). Oxygen minimum zones (OMZs) in the modern ocean. *Prog. Oceanogr.* 80 (3), 113–128. doi:10.1016/j.pocean.2008.08.001

Peng, X. N. (2015) "Nitrogen cycling in strong redox gradients of marine environments," in *Oceanic oxygen minimum zones and salt marsh sediments [Dissertation: pub. No. 3737408]*. Princeton University.

Pi, D. H., Jiang, S. Y., Luo, L., Yang, J. H., and Ling, H. F. (2014). Depositional environments for stratiform witherite deposits in the Lower Cambrian black shale sequence of the Yangtze Platform, southern Qinling region, SW China: evidence from redox-sensitive trace element geochemistry. *Palaeogeogr. Palaeoclimatol. Palaeoecol.* 398, 125–131. doi:10.1016/j.palaeo.2013.09.029

Pisarzowska, A., Rakociński, M., Marynowski, L., Szczerba, M., Thoby, M., Paszkowski, M., et al. (2020). Large environmental disturbances caused by magmatic activity during the Late Devonian Hangenberg Crisis. *Glob. Planet. Change* 190, 103155. doi:10.1016/j.gloplacha.2020.103155

Poole, F. G. (1973). Flysch deposits of antler foreland basin, western United States: abstract. *AAPG Bull.* 57 (4), 800–801. doi:10.1306/83d90c32-16c7-11d7-8645000102c1865d

Qie, W., Wang, X.-D., Zhang, X., Ji, W., Grossman, E. L., Huang, X., et al. (2016). Latest Devonian to earliest Carboniferous conodont and carbon isotope stratigraphy of a shallow-water sequence in South China. *Geol. J.* 51 (6), 915–935. doi:10.1002/gj.2710

Rakociński, M., Marynowski, L., Pisarzowska, A., Bełdowski, J., Siedlewicz, G., Zatoń, M., et al. (2020). Volcanic-related methylmercury poisoning as the possible driver of the End-Devonian mass extinction. *Sci. Rep.* 10 (1), 7344. doi:10.1038/s41598-020-64104-2

Redfield, A. C. (1958). The biological control of chemical factors in the environment. *Am. Sci.* 46 (3), 230A–221A. Available at: http://www.jstor.org/stable/27827150.

Reyes-Mendoza, O., Herrera-Silveira, J., Mariño-Tapia, I., Enriquez, C., and Largier, J. L. (2019). Phytoplankton blooms associated with upwelling at Cabo Catoche. *Cont. Shelf Res.* 174, 118–131. doi:10.1016/j.csr.2018.12.015

Richards, B. C. (1989). Uppermost Devonian and Lower Carboniferous stratigraphy sedimentation and diagenesis in the southwestern district of Mackenzie and southeastern Yukon territory. *En. Mines, Res. Can*. doi:10.4095/127662

Richards, B. C., and Higgins, A. C. (1988). Devonian-Carboniferous boundary beds of the palliser and Exshaw formations at Jura Creek, Rocky mountains, southwestern Alberta. *Geol*.

Richards, B. C. B., E, W., Henderson, C. M., Higgins, A. C., Johnston, D. I., Mamet, B., et al. (1994). Uppermost Devonian (Famennian) and lower Carboniferous (Tournaisian) at Jura Creek and mount Rundle, southwestern Alberta. *Geol. Sur. Can. Open File*, 2866.

Robison, V. D. (1995). "The Exshaw Formation: a Devonian/Mississippian hydrocarbon source in the western Canada basin," in *Petrol. Source rocks*. Editor B. J. Katz (Springer Berlin Heidelberg), 9–24.

Romaniello, S., and Derry, L. (2010). Validation of an intermediate-complexity model for simulating marine biogeochemistry under anoxic conditions in the modern Black Sea. *Geochem. Geophys. Geosyst.* 11. doi:10.1029/2009GC002712

Ross, D. J. K., and Bustin, R. M. (2008). Characterizing the shale gas resource potential of Devonian–Mississippian strata in the Western Canada sedimentary basin: application of an integrated formation evaluation. *AAPG Bull.* 92 (1), 87–125. doi:10.1306/09040707048

Ruebsam, W., and Schwark, L. (2023). Phytoplankton dynamics and nitrogen cycling during Oceanic Anoxic Event 2 (Cenomanian/Turonian) in the upwelling zone of the NE proto-North Atlantic. *Glob. Planet. Change* 224, 104117. doi:10.1016/j.gloplacha.2023.104117

Saltzman, M. R. (2005). Phosphorus, nitrogen, and the redox evolution of the Paleozoic oceans. *Geology* 33 (7), 573–576. doi:10.1130/g21535.1

Savoy, L. E. (1990). *Sedimentary record of Devonian-Mississippian carbonate and black shale systems, southernmost Canadian Rockies and adjacent Montana: facies and processes*. [Dissertation]. Syracuse University.

Savoy, L. E. (1992). Environmental record of Devonian-Mississippian carbonate and low-oxygen facies transitions, southernmost Canadian Rocky Mountains and northwesternmost Montana. *GSA Bull.* 104 (11), 1412–1432. doi:10.1130/0016-7606(1992)104<1412:ERODMC>2.3.CO;2

Schmoker, J. W., and Hester, T. C. (1983). Organic carbon in Bakken Formation, United States portion of Williston Basin. *AAPG Bull.* 67 (12), 2165–2174. doi:10.1306/AD460931-16F7-11D7-8645000102C1865D

Scholze, F., and Gess, R. W. (2017). Oldest known naiaditid bivalve from the high-latitude Late Devonian (Famennian) of South Africa offers clues to survival strategies following the Hangenberg mass extinction. *Palaeogeogr. Palaeoclimatol. Palaeoecol.* 471, 31–39. doi:10.1016/j.palaeo.2017.01.018

Schönfeld, J., Kuhnt, W., Erdem, Z., Flögel, S., Glock, N., Aquit, M., et al. (2015). Records of past mid-depth ventilation: Cretaceous Ocean Anoxic Event 2 vs. recent oxygen minimum zones. *Biogeosc* 12 (4), 1169–1189. doi:10.5194/bg-12-1169-2015

Shizuya, A., Oba, M., Ando, T., Ogata, Y., Takashima, R., Nishi, H., et al. (2020). Variations in trace elements, isotopes, and organic geochemistry during the Hangenberg Crisis, Devonian–Carboniferous transition, northeastern Vietnam. *Isl. Arc* 29 (1), e12337. doi:10.1111/iar.12337

Sigman, D. M., Altabet, M. A., McCorkle, D. C., Francois, R., and Fischer, G. (1999). The $\delta^{15}N$ of nitrate in the southern ocean: consumption of nitrate in surface waters. *Glob. Biogeochem. Cycles* 13 (4), 1149–1166. doi:10.1029/s1999GB900038

Sigman, D. M., Casciotti, K. L., Andreani, M., Barford, C., Galanter, M., and Böhlke, J. K. (2001). A bacterial method for the nitrogen isotopic analysis of nitrate in seawater and freshwater. *Anal. Chem.* 73 (17), 4145–4153. doi:10.1021/ac010088e

Smith, M. G., and Bustin, R. M. (2000). Late Devonian and Early Mississipian Bakken and Exshaw black shale source rocks, Western Canada Sedimentary Basin: a sequence stratigraphic interpretation. *AAPG Bull.* 84, 94–960. doi:10.1306/a9673b76-1738-11d7-8645000102c1865d

Smith, M. G., Bustin, R. M., and Caplan, M. L. (1995). Sequence stratigraphy of the Bakken and Exshaw formations: a continuum of black shale formations in the Western Canada Sedimentary Basin. *Seventh Int. Willist. Basin Symp. MTGS-AAPG*, 399–409.

Smith, M. T., Dickinson, W. R., and Gehrels, G. E. (1993). Contractional nature of Devonian-Mississippian Antler tectonism along the North American continental margin. *Geology* 21 (1), 21–24. doi:10.1130/0091-7613(1993)021<0021:Cnodma>2.3.Co;2

Stief, P. (2013). Stimulation of microbial nitrogen cycling in aquatic ecosystems by benthic macrofauna: mechanisms and environmental implications. *Biogeosc. Discuss.* 10, 7829–7846. doi:10.5194/bg-10-7829-2013

Stoyles, K. C., Davies, G. R., and Spila, M. V. (2011). *Regional stratigraphic study of the exshaw/bakken formations: insights from sedimentology and ichnology recovery –cspg CSEG CWLS convention*.

Taylor, S. R., and McLennan, S. M. (1985). *The Continental Crust; its composition and evolution; an examination of the geochemical record preserved in sedimentary rocks*. Oxford: Blackwell, 312.

Thunell, R. C., Sigman, D. M., Muller-Karger, F., Astor, Y., and Varela, R. (2004). Nitrogen isotope dynamics of the Cariaco Basin, Venezuela. *Glob. Biogeochem. Cycles* 18 (3). doi:10.1029/2003GB002185

Tribovillard, N., Algeo, T. J., Lyons, T., and Riboulleau, A. (2006). Trace metals as paleoredox and paleoproductivity proxies: an update. *Chem. Geol.* 232, 12–32. doi:10.1016/j.chemgeo.2006.02.012

Tuite, M. L., Williford, K. H., and Macko, S. A. (2019). From greenhouse to icehouse: nitrogen biogeochemistry of an epeiric sea in the context of the oxygenation of the Late Devonian atmosphere/ocean system. *Palaeogeogr. Palaeoclimatol. Palaeoecol.* 531, 109204. doi:10.1016/j.palaeo.2019.05.026

Tyrrell, T. (1999). The relative influences of nitrogen and phosphorus on oceanic primary production. *Nature* 400 (6744), 525–531. doi:10.1038/22941

Uveges, B. T., Junium, C. K., Boyer, D. L., Cohen, P. A., and Day, J. E. (2019). Biogeochemical controls on black shale deposition during the Frasnian-Famennian biotic crisis in the Illinois and Appalachian Basins, USA, inferred from stable isotopes of nitrogen and carbon. *Palaeogeogr. Palaeoclimatol. Palaeoecol.* 531, 108787. doi:10.1016/j.palaeo.2018.05.031

Uveges, B. T., and Pearson, A. (2023). Ammonium "nutrient capacitor" model for $\delta^{15}N$ signatures associated with marine anoxic events. *Geology* 51, 1132–1136. doi:10.1130/G51527.1

Van Cappellen, P., and Ingall, E. D. (1996). Redox stabilization of the atmosphere and oceans by phosphorus-limited marine productivity. *Science* 271 (5248), 493–496. doi:10.1126/science.271.5248.493

Velinsky, D. J., and Fogel, M. L. (1999). Cycling of dissolved and particulate nitrogen and carbon in the Framvaren Fjord, Norway: stable isotopic variations. *Mar. Chem.* 67 (3), 161–180. doi:10.1016/S0304-4203(99)00057-2

Velinsky, D. J., Fogel, M. L., Todd, J. F., and Tebo, B. M. (1991). Isotopic fractionation of dissolved ammonium at the oxygen-hydrogen sulfide interface in anoxic waters. *Geophys. Res. Lett.* 18 (4), 649–652. doi:10.1029/91GL00344

Vernon, M. R. (2001). *Petrology, geochemistry, diagenesis and depositional environment of the upper devonian - lower carboniferous Exshaw Formation, northwestern Alberta [dissertation: pub. No. 3077]*. University of Windsor.

Visy, J. M. (2022). *Stratigraphic partitioning and reservoir distribution of the late devonian to early mississippian Exshaw Formation, western Canada Sedimentary Basin*. Baylor University. [Master's Thesis].

Voss, M., Dippner, J. W., and Montoya, J. P. (2001). Nitrogen isotope patterns in the oxygen-deficient waters of the eastern tropical north Pacific Ocean. *Deep-Sea Res.* 48 (8), 1905–1921. doi:10.1016/S0967-0637(00)00110-2

Waser, N. A. D., Harrison, P. J., Nielsen, B., Calvert, S. E., and Turpin, D. H. (1998). Nitrogen isotope fractionation during the uptake and assimilation of nitrate, nitrite, ammonium, and urea by a marine diatom. *Limnol. Oceanogr.* 43 (2), 215–224. doi:10.4319/lo.1998.43.2.0215

Werne, J. P., Sageman, B. B., Lyons, T. W., and Hollander, D. J. (2002). An integrated assessment of a "type euxinic" deposit: evidence for multiple controls on black shale deposition in the middle Devonian Oatka Creek formation. *Am. J. Sci.* 302 (2), 110–143. doi:10.2475/ajs.302.2.110

Zaitlin, B. A. (2011). *The Alberta bakken: a potential new, unconventional tight oil resource play recovery - 2011 cspg cseg cwls convention*.

Zehr, J. P., and Ward, B. B. (2002). Nitrogen cycling in the ocean: new perspectives on processes and paradigms. *Appl. Environ. Microbio.* 68(3), 1015–1024. doi:10.1128/AEM.68.3.1015-1024.2002

Zhang, F., Dahl, T. W., Lenton, T. M., Luo, G., Shen, S.-z., Algeo, T. J., et al. (2020). Extensive marine anoxia associated with the late devonian Hangenberg crisis. *Earth Planet. Sci. Lett.* 533, 115976. doi:10.1016/j.epsl.2019.115976

Zhang, X., Joachimski, M. M., and Gong, Y. (2021). Late Devonian greenhouse-icehouse climate transition: new evidence from conodont $\delta^{18}O$ thermometry in the eastern Palaeotethys (Lali section, South China). *Chem. Geol.* 581, 120383. doi:10.1016/j.chemgeo.2021.120383

Zhou, X., Thomas, E., Winguth, A. M. E., Ridgwell, A., Scher, H., Hoogakker, B. A. A., et al. (2016). Expanded oxygen minimum zones during the late Paleocene-early Eocene: hints from multiproxy comparison and ocean modeling. *Paleoceanogr* 31 (12), 1532–1546. doi:10.1002/2016PA003020